

A multiscalar global evaluation of the impact of ENSO on droughts

Sergio M. Vicente-Serrano,¹ Juan I. López-Moreno,¹ Luis Gimeno,² Raquel Nieto,² Enrique Morán-Tejeda,¹ Jorge Lorenzo-Lacruz,¹ Santiago Beguería,³ and Cesar Azorin-Molina¹

Received 30 March 2011; revised 3 August 2011; accepted 3 August 2011; published 20 October 2011.

[1] In this study we analyzed the influence of the El Niño–Southern Oscillation (ENSO) phenomenon on drought severity at the global scale. A unique aspect of the analysis is that the ENSO influence was quantified using a multiscalar drought indicator, which allowed assessment of the role of the ENSO phases on drought types affecting various hydrological, agricultural and environmental systems. The study was based on ENSO composites corresponding to El Niño and La Niña phases, which were obtained from the winter El Niño 3.4 index for the period 1901–2006. Drought was identified in a multiscalar way using the Standardized Precipitation Evapotranspiration Index (SPEI) and the global SPEIbase data set. The study revealed the differing impacts of the El Niño and La Niña phases on drought severity, the time scales of droughts, and the period of the year when the ENSO phases explained drought variability worldwide. In large areas of America and eastern Europe the role of ENSO events were evident at the shortest time scales (1–3 months) at the beginning of events, but in areas of South Africa, Australia and Southeast Asia the effects were more obvious some months later, and at longer time scales. We also identified areas where severe drought conditions are associated with more than 70% of ENSO events. The persistence of the drought signal at longer time-scales (e.g., 6- or 12-months) is not directly determined by the atmospheric circulation response to the SST anomalies, since the SPEI anomalies will be caused by the cumulative dry conditions in some specific months. Knowledge of how these effects differ as a function of the El Niño and La Niña phases, and how they propagate throughout the drought time scales could aid in the prediction of the expected drought severity associated with the ENSO. Lags detected during the study may help forecasting of dry conditions in some regions up to one year before their occurrence.

Citation: Vicente-Serrano, S. M., J. I. López-Moreno, L. Gimeno, R. Nieto, E. Morán-Tejeda, J. Lorenzo-Lacruz, S. Beguería, and C. Azorin-Molina (2011), A multiscalar global evaluation of the impact of ENSO on droughts, *J. Geophys. Res.*, 116, D20109, doi:10.1029/2011JD016039.

1. Introduction

[2] The El Niño–Southern Oscillation (ENSO) phenomenon is one of the main sources of variability in the Earth's climate [Trenberth, 1997; Kiladis and Díaz, 1989; Halpert and Ropelewski, 1992; Philander and Fedorov, 2003]; the extremes of this atmosphere–ocean coupled mode are known as the El Niño and La Niña phases. El Niño phases correspond to ENSO events during which pressure differences across the tropical Pacific Ocean are reduced, and sea surface temperature (SST) anomalies are positive in the central and eastern tropical Pacific Ocean [Philander, 1990]. La Niña phases correspond to ENSO events characterized

by cold SST and an enhanced sea level pressure gradient from west to east across the tropical Pacific Ocean. These anomalous phases affect the temperature of the atmosphere, and the surface and vertical displacement of wind flows and moisture [Rasmusson and Carpenter, 1982].

[3] Many studies have shown a close relationship between ENSO phenomena and climate variability in tropical and subtropical regions [e.g., Ropelewski and Halpert, 1986, 1987; Kiladis and Diaz, 1989; Redmond and Koch, 1991]. During El Niño (La Niña) phases there is increased (decreased) precipitation in the south Pacific Ocean, whereas dry (wet) conditions occur in Australia, Southeast Asia, South Africa and northern South America [Smith and Ropelewski, 1997; Cordery and McCall, 2000; Hendon, 2003; Rouault and Richard, 2005; Brown et al., 2009; Nel, 2009; Espinoza Villar et al., 2009; Kothawale et al., 2010].

[4] The ENSO influence on precipitation is not restricted to the Pacific Ocean. Thus, New et al. [2001] estimated that the ENSO phenomenon causes 6.3% of precipitation variance at

¹Instituto Pirenaico de Ecología, CSIC, Zaragoza, Spain.

²Environmental Physics Laboratory, Universidade de Vigo, Ourense, Spain.

³Estación Experimental de Aula Dei, CSIC, Zaragoza, Spain.

the global scale, and also helps explain the climate variability of northern hemisphere regions, mainly in the north Pacific Ocean and North America [Díaz and Kiladis, 1992; Schonher and Nicholson, 1989; Halpert and Ropelewski, 1992; Ropelewski and Halpert, 1996; Trenberth and Guillemot, 1996; Mo and Schemm, 2008], on the European continent [Lloyd-Hughes and Saunders, 2002; Brönnimann et al., 2004; Brönnimann, 2007], and in Turkey [Karabörk et al., 2005; Karabörk and Kahya, 2009], the Sahel [Janicot et al., 1996, 2001] and large areas of central Asia [Mariotti, 2007; Nazemosadat and Ghasemi, 2004].

[5] Current interest in climate responses to variations in atmospheric circulation is mainly focused on the occurrence of extreme events (e.g., floods, droughts, heat waves) that cause major environmental, social and economic damage. Among natural hydroclimatic hazards, drought is the most damaging because it causes major economic losses [Meehl et al., 2000; United Nations, 2008], famine [Obasi, 1994; Nicholson, 2001] and negative environmental impacts [e.g., Ciais et al., 2005; Breshears et al., 2005].

[6] Droughts are very difficult complex natural hazards to identify, monitor and analyze because of problems associated with objectively quantifying their characteristics in terms of intensity, magnitude, duration and spatial extent. Consequently, determining drought mechanisms is problematic and it is very difficult to establish their onset, extent and cessation. Moreover, drought is a multiscale phenomenon, which adds much complexity to any analysis. McKee et al. [1993] clearly illustrated these characteristics of droughts through consideration of usable water resources, including soil moisture, groundwater, snowpack, river discharges and reservoir storages. The time period from the arrival of water inputs to the availability of a given usable water resource varies considerably. Thus, the time scale over which water deficits accumulate becomes extremely important, and functionally separates hydrological, environmental, agricultural and other types of droughts. Thus, the response of crops, natural vegetation and hydrological systems to drought conditions can vary markedly as a function of the time scale [Ji and Peters, 2003; Vicente-Serrano and López-Moreno, 2005; Patel et al., 2007; Vicente-Serrano, 2007; Khan et al., 2008; Lorenzo-Lacruz et al., 2010; Quiring and Ganesh, 2010]. This multi-temporal character makes it difficult to identify clear relationships between atmospheric circulation patterns and drought variability. This difficulty is exacerbated by the lags that commonly occur in the response of climatic conditions to atmospheric circulation events, such as El Niño and La Niña.

[7] Few studies have quantified the influence of ENSO phases on droughts using drought indices, and relatively few regions of the world have been studied. These regions are mainly in the USA [Piechota and Dracup, 1996; Rajagopalan et al., 2000; Balling and Goodrich, 2007; Mo and Schemm, 2008; Mo et al., 2009], but also in Indonesia [D'Arrigo and Wilson, 2008], Canada [Shabbar and Skinner, 2004], New Zealand [Fowler and Adams, 2004], South Africa [Rouault and Richard, 2005], Iran [Nazemosadat and Ghasemi, 2004] and the Iberian Peninsula [Vicente-Serrano, 2005].

[8] Some studies have analyzed the impact of ENSO on droughts at the global scale. Dai et al. [2004] developed a global data set of the Palmer Drought Severity Index (PDSI)

and showed that between 1870 and 2002 the pattern of drought variability representing the drought evolution in large regions of North America and central Eurasia was strongly correlated to the ENSO. Apipattanavis et al. [2009] also related the global PDSI with the ENSO, and showed a strong relationship in the southwestern and northwestern United States, South Africa, northeastern Brazil, central Africa, the Indian subcontinent and Australia. Sheffield et al. [2009] recently used an infiltration capacity model to quantify the global occurrence of droughts for the period 1950–2000. They found robust relationships between the surface area of the world affected by drought and the ENSO variability. While useful and informative, these global studies did not consider the impact of ENSO on drought at different time scales, and thus its impact on various sub-systems of the hydrological cycle.

[9] Vicente-Serrano [2005] used a multiscale drought index (the Standardized Precipitation Index) to show that the influence of the El Niño and La Niña phases varies widely across time scales in the Iberian Peninsula; this approach is essential in accurately quantifying the wide variety of impacts related to ENSO variability. Thus, when the atmospheric mechanisms of droughts are studied, differing drought time scales must be considered to have a wide perspective of the hazard implications [López-Moreno and Vicente-Serrano, 2008].

[10] This study is the first global multiscale analysis of the ENSO impact on droughts. The purpose was to provide a general picture of drought conditions at various time scales associated with warm (El Niño) and cold (La Niña) ENSO events and the associated physical mechanisms. Establishing robust relationships between the ENSO and the evolution of drought is of great relevance because ENSO is the main source of atmospheric circulation variability at a global scale. Such knowledge will facilitate improved prediction of droughts [e.g., Stone et al., 1996; Cordery and McCall, 2000], which will enhance the performance of existing drought early warning and monitoring systems [Svoboda et al., 2002, 2004].

2. Methods

2.1. Identification of ENSO Events

[11] El Niño phenomenon is very complex not only in terms of temporal variability but also in its spatial pattern. For example, Fu et al. [1986] identified three types of El Niño phenomena according to the spatial distribution of the sea surface temperature anomalies in the South Pacific area. Kahya and Dracup [1994] analyzed the influence of type I El Niño events (summer El Niño) in the southwest of the United States and showed noticeable differences regarding to the impact of the winter El Niño events. Recently, Ashok and Yamagata [2009] have also showed a new spatial mode of ENSO, named El Niño Modoki that shows a different spatial configuration regarding common winter ENSO events. The results presented in the paper depict a typical (mean) ENSO cycle based on winter composites. Although each ENSO cycle is different and it is difficult to predict its evolution even after its inception, most of the ENSO events peak in winter months.

[12] Composites based on ENSO events are commonly used to analyze the nonlinear influence of the ENSO on

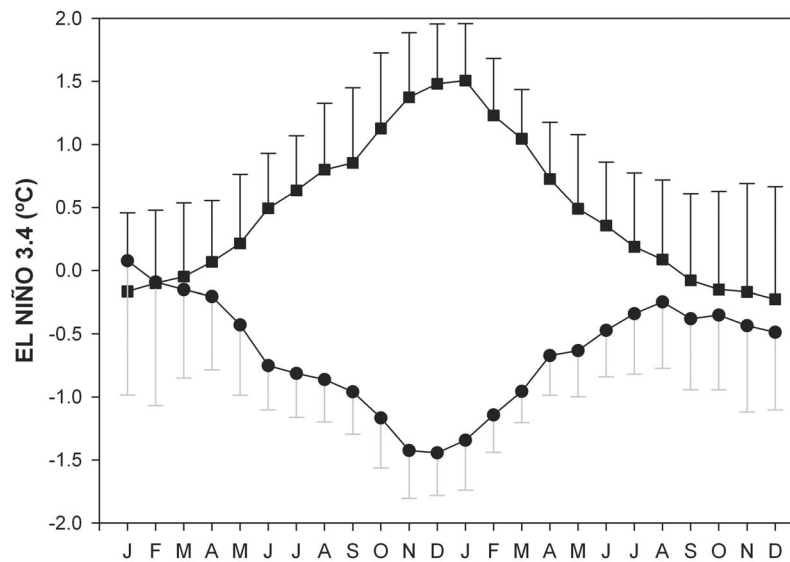


Figure 1. Monthly SST anomalies (in degrees) corresponding to the phases of the winter El Niño (squares) and La Niña (circles). The monthly means were computed for each time series for the period 1971–2000. These means were then subtracted from their respective time series for the entire data set (1901–2006).

world climate [Smith and Ropelewski, 1997; Philip and van Oldenborgh, 2009] because the composite warm event ENSO anomalies are not the exact inverse of their cold event counterparts [Hoerling *et al.*, 1997].

[13] There is general agreement on use of the El Niño 3.4 to monitor ENSO phenomena and to identify its extreme phases. This index was proposed by Trenberth and Hoar [1996], based on the SST in two selected Pacific Ocean areas, which are key regions for ENSO. The index has been widely applied to monitoring of the effect of ENSO on the global climate system, and also used to identify the extreme phases of the ENSO [Trenberth, 1997]. In this study the El Niño and La Niña events were identified using the winter (December–February) El Niño 3.4 index between 1901 and 2006, obtained from the Hadley Centre Sea Surface Temperature data set [Rayner *et al.*, 2003]. El Niño events were defined by a winter El Niño 3.4 index >1 , and La Niña events were defined by an index <-1 . Based on these criteria the winters of 1903, 1906, 1912, 1919, 1926, 1931, 1941, 1958, 1966, 1969, 1973, 1983, 1987, 1992, 1995, 1998 and 2003 were classified as El Niño, and the winters of 1910, 1917, 1934, 1943, 1950, 1951, 1956, 1971, 1974, 1976, 1985, 1989, 1999 and 2000 were classified as La Niña. By convention the El Niño and La Niña years were defined as those that correspond to the year when records the months of January and February of the event. The month of December therefore corresponded to the year prior to the ENSO event.

[14] We plotted the average and standard deviation values of the El Niño 3.4 index for the entire year of El Niño and La Niña events, and also for the previous year (Figure 1). Trenberth [1997] carried out an extensive analysis of the ENSO extreme phases using the El Niño 3.4 index, and showed that most events began between March and September. Figure 1 shows that the greatest anomalies for both

events (El Niño and La Niña) occurred during the winter months (November–January), but the anomalies in SSTs associated with the events commenced in May of the previous year and extended to May–June in the year of the event. Thus, for La Niña and El Niño phases SST anomalies <-0.75 and >0.5 , respectively, were recorded from June of the previous year. Therefore, as the ENSO phases were recorded in the winter months and large anomalies in the SST occurred some months prior to and following these phases, it is reasonable to predict the early influence of ENSO events on drought conditions in some regions, with implications at various time scales. For this reason the drought analyses encompassed the year of the event and most of the preceding year.

2.2. Drought Data Set

[15] To identify drought conditions we used the Standardized Precipitation Evapotranspiration Index (SPEI), which can be calculated at different time scales and considers the combined effects of precipitation and temperature. The SPEI combines the sensitivity of the Palmer Drought Severity Index (PDSI) to changes in evaporation demand (caused by temperature fluctuations and trends) with the multitemporal nature of the Standardized Precipitation Index (SPI). Further details on the drought indicator have been provided by Vicente-Serrano *et al.* [2010a].

[16] The drought data set used (the SPEIbase, which is based on SPEI) covers the entire Earth at time scales from 1 to 48 months at a spatial resolution of 0.5° , providing temporal coverage for the period 1901–2006. This data set combines improved spatial resolution with the operative capability of previous gridded drought data sets based on the PDSI, and enables identification of various drought types. Details of the SPEIbase have been reported by Vicente-Serrano *et al.* [2010b] and Beguería *et al.* [2010]. In this

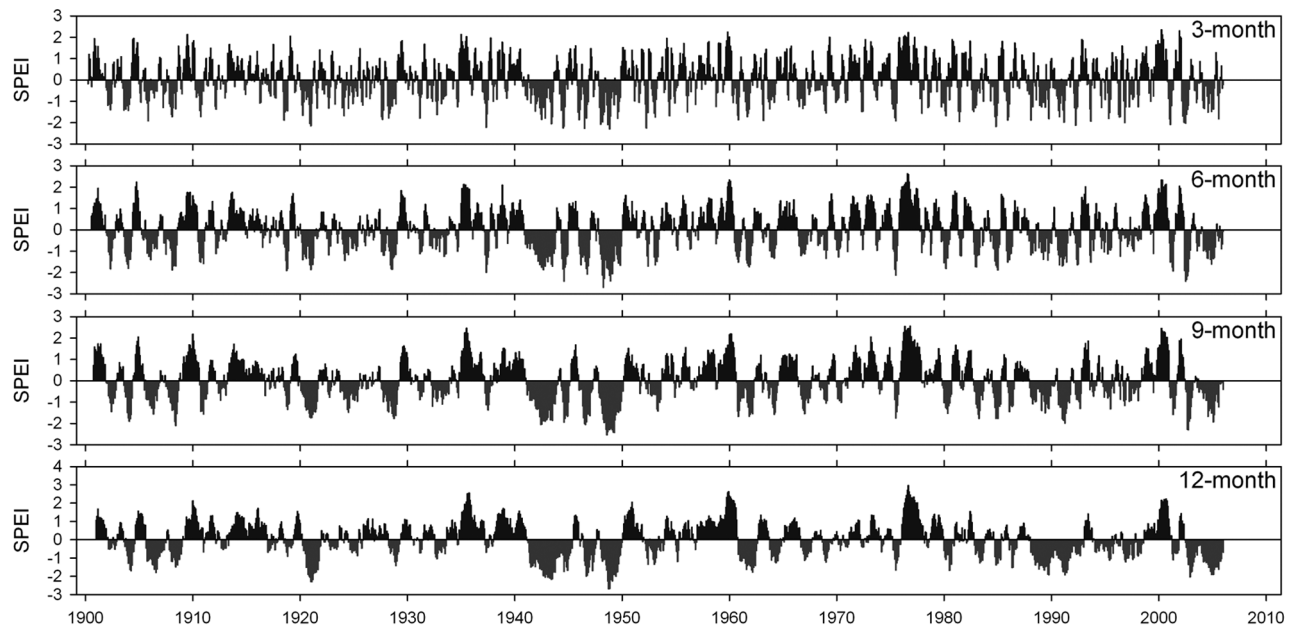


Figure 2. Evolution of the 3-, 6-, 9- and 12-month SPEI in central France (46.5°N, 8°E).

study we used time scales from 1 to 12 months to isolate the annual effects of the ENSO events.

[17] Figure 2 provides an example of the evolution of the SPEI at time scales of 3, 6, 9 and 12 months in an area of central France (46.5°N, 8°E). At the shorter time scales (e.g., 3 months) there is a continuous alternation of short dry and humid periods. At longer time scales (e.g., 12 months) droughts were less frequent but lasted longer. Numerous scientific studies have shown that particular systems and regions can respond to drought conditions at very different time scales. In terms of water resources, *Vicente-Serrano and López-Moreno* [2005] showed that the response of river discharges and reservoir storages to different drought time scales in mountainous catchments can be diverse (1–2 months for river discharges and 8–10 for reservoir storages). *Szalai et al.* [2000] also showed that water stored in reservoirs in Hungary responded to longer time scales (5 to 24 months) than streamflows (2 to 6 months). Large differences were also observed using groundwater data [e.g., *Khan et al.*, 2008; *Fiorillo and Guadagno*, 2010; *Vidal et al.*, 2010]. A similar fact can be observed for other systems, such as crops or natural vegetation. For example, *Vicente-Serrano* [2007] showed that vegetation activity in northeast Spain, monitored by means of remote sensing, shows a contrasted response to drought, but the time-scales at which the drought indices are calculated play a major role when determining the impacts. *Ji and Peters* [2003] also showed in the North American prairies that different grassland communities respond very differently to drought as a function of the time scale. *Quiring and Ganesh* [2010] have obtained similar results in Texas. These results stress the need of analyzing droughts on different time-scales.

2.3. Analysis

[18] An empirical methodology similar to that adopted by *Ropelewski and Halpert* [1986, 1987, 1996], *Piechota and*

Dracup [1996] and *Karabörk and Kahya* [2003] was used to determine the impact of El Niño and La Niña years on global drought conditions. The approach followed that of a previous study [*Vicente-Serrano*, 2005] that analyzed the impact of ENSO events on droughts in the Iberian Peninsula. Average SPEI anomalies at various time scales were calculated for El Niño and La Niña years, and the year preceding.

[19] To determine whether the SPEI at different time scales reflected significant humid or dry conditions during El Niño or La Niña phases, the Wilcoxon-Mann-Whitney test was used [*Siegel and Castelan*, 1988]. The Wilcoxon-Mann-Whitney test is based on ranks that do not require normally distributed samples, and is slightly less powerful than parametric tests including the t-test [*Helsel and Hirsch*, 1992]. The SPEI values in each of the months of El Niño/La Niña years were compared with the values of the SPEI for the months of normal years and those with the opposite sign. Thus, to determine the role of the El Niño years the SPEI values during La Niña years were added to the SPEI values during normal years, and vice versa. The significance level was defined as $\alpha < 0.05$.

2.4. Analysis of the Atmospheric Driving Mechanisms

[20] In order to analyze the possible physical mechanisms and atmospheric patterns that propagate the El Niño and La Niña signal on droughts worldwide we obtained the average standardized anomalies of global Sea Surface Temperature (SST), Sea Level Pressure (SLP) and 500 hPa geopotential heights corresponding to the months of El Niño and La Niña phases. For the SST, the Extended Reconstruction Sea Surface Temperature (ERSST) v3.b data set at a resolution of 2° degrees was used [*Smith and Reynolds*, 2004]. The SLP and 500 hPa monthly fields were obtained from the Twentieth Century Reanalysis at a

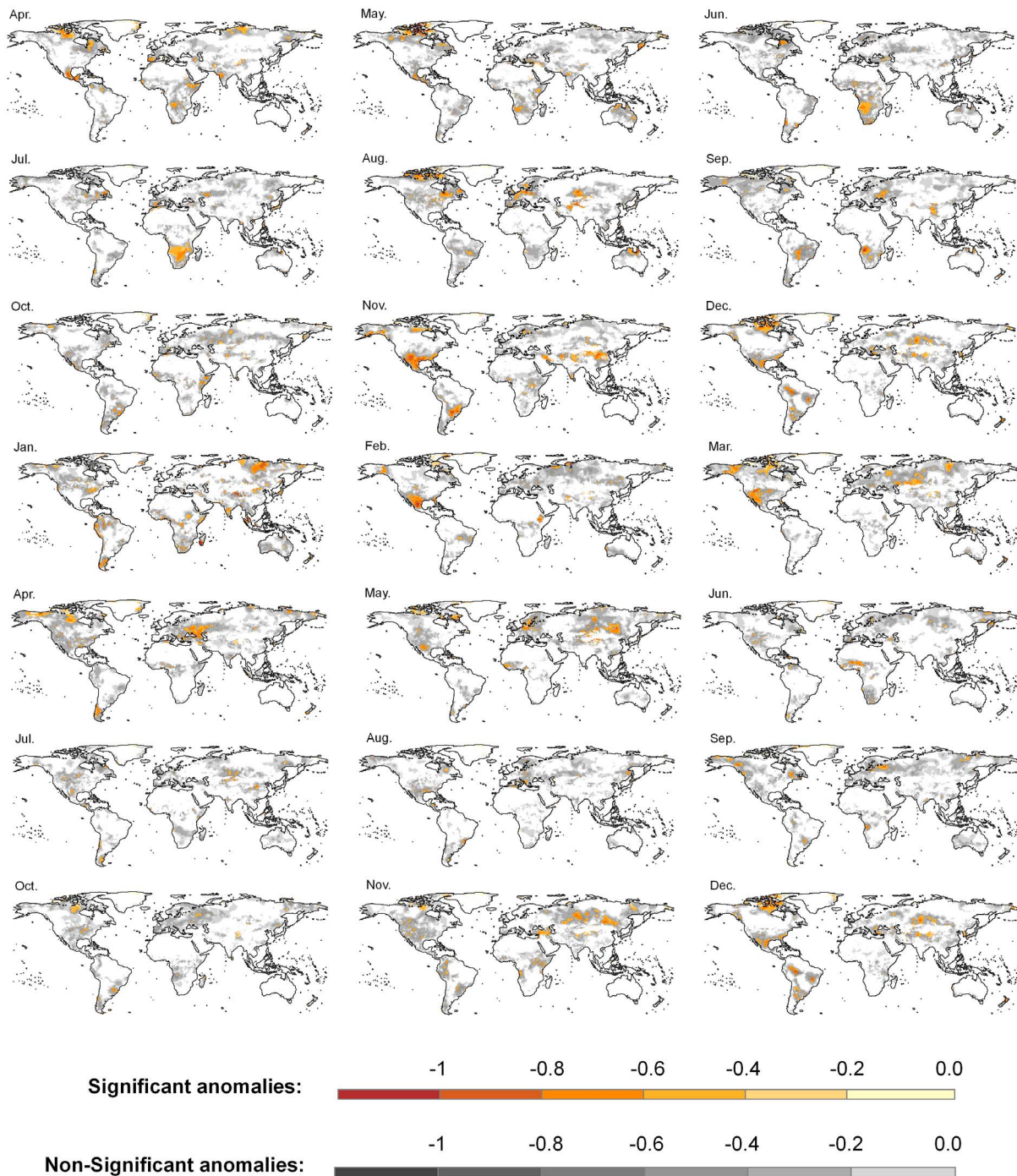


Figure 3. Spatial distribution of the average 1-month SPEI composite anomalies during La Niña years and the years preceding. Orange/reds identify areas in which significant differences in the SPEI average were found between the La Niña years and other years. Greys identify negative but non-significant anomalies.

resolution of 2° for the period 1901–2006 [Compo *et al.*, 2011].

3. Results

3.1. La Niña Events and Multiscalar Droughts Globally

[21] Figure 3 shows the monthly average anomalies of the 1-month SPEI during years under La Niña conditions, and

from April of the previous year, when negative anomalies in the moisture conditions had been identified. The possible positive anomalies are not shown because the study focus was on droughts associated with ENSO events. Major negative moisture anomalies over large areas of the world were evident at the 1-month time scale from the middle of the preceding year. Thus, in June and July of the year prior to the La Niña event dry conditions were recorded in areas

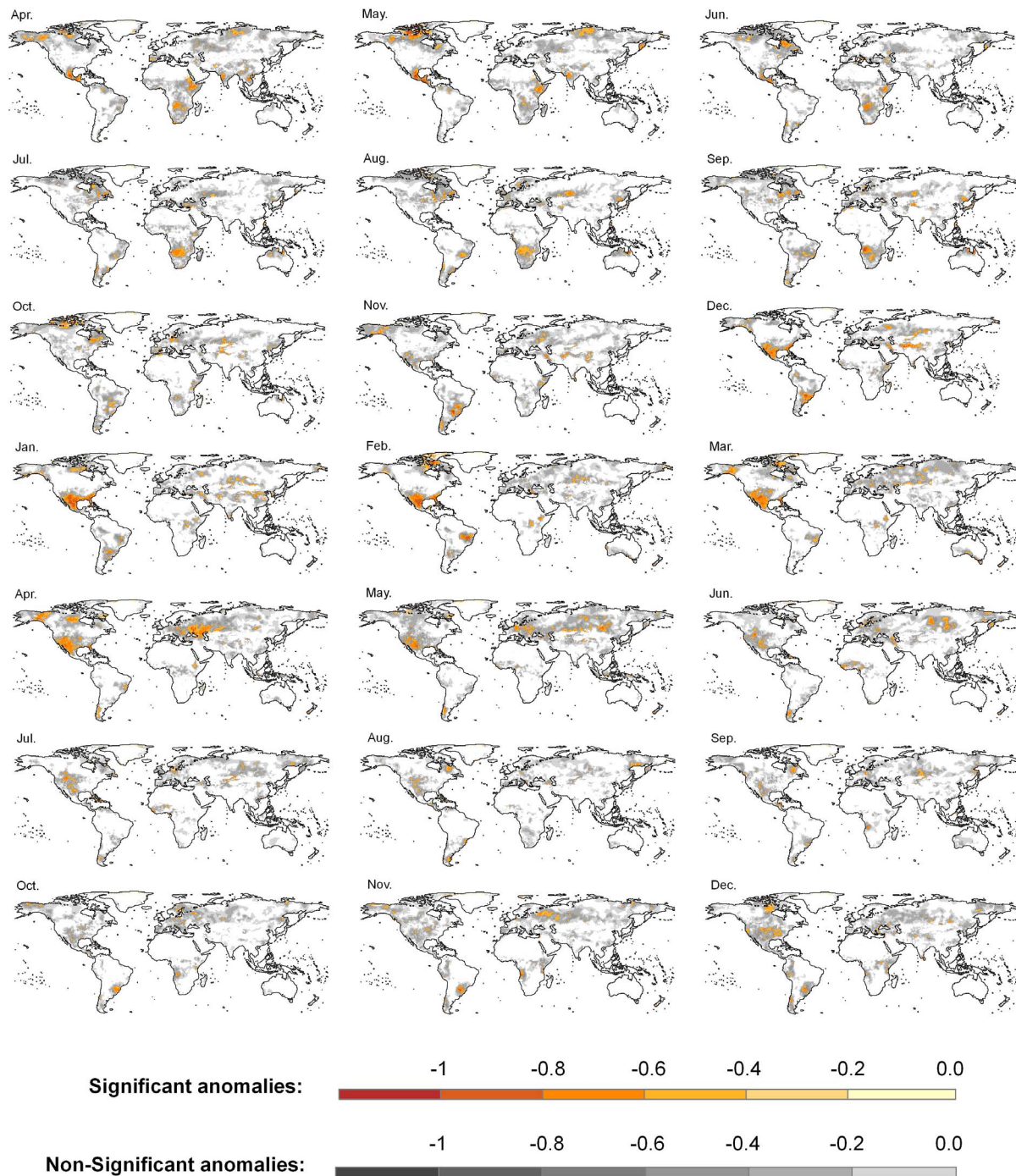


Figure 4. Spatial distribution of the average 3-month SPEI composite anomalies during La Niña years and the years preceding. Orange/reds identify areas in which significant differences in the SPEI average were found between the La Niña years and other years. Greys identify negative but non-significant anomalies.

of South Africa, Europe and North America, but from November of the previous year to March of the La Niña year the main negative anomalies occurred on the American continent. The major anomalies detected globally occurred in the southern USA/northern Mexico region. From November to March the anomalies continuously covered large areas of this region, but even until June patchy areas with significant negative anomalies were detected during La

Niña years. The effects were also evident in some regions of South America from November to January, and in parts of Eurasia.

[22] At the time scale of 3 months most of the drought conditions associated with La Niña phases, which had been observed in the regions with negative anomalies at the time scale of 1 month, were confirmed and propagated over longer periods (Figure 4). For example, in regions of South

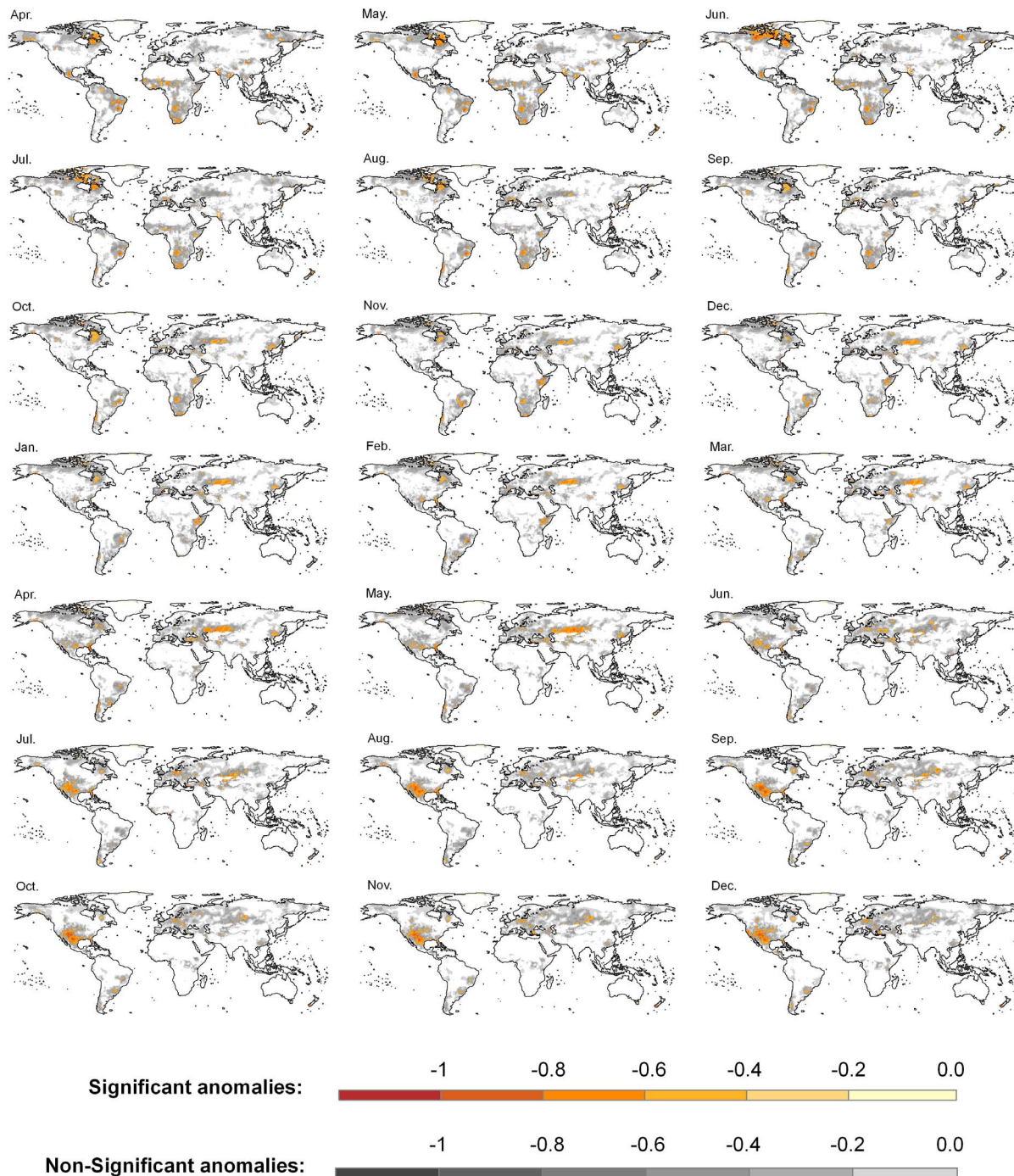


Figure 5. Spatial distribution of the average 12-month SPEI composite anomalies during La Niña years and the years preceding. Orange/reds identify areas in which significant differences in the SPEI average were found between the La Niña years and other years. Greys identify negative but non-significant anomalies.

Africa significant negative anomalies were identified from June to September of the year prior to the La Niña phase. Nevertheless, the effect was most evident in southern USA/northern Mexico, where strong negative and significant anomalies in the SPEI were found for La Niña events. Negative anomalies were also found in areas of northern Argentina and southern Brazil from November in the year prior to a La Niña event to January in the event year.

Moreover, in eastern Europe and western Russia negative anomalies were clearly evident from March to May of La Niña years.

[23] At the 12-month time scale the negative SPEI anomalies were confirmed in terms of duration and magnitude (Figure 5). It is notable that at this time scale drought conditions were identified earlier in southern Russia and Kazakhstan (from March to May) than in the southern USA/

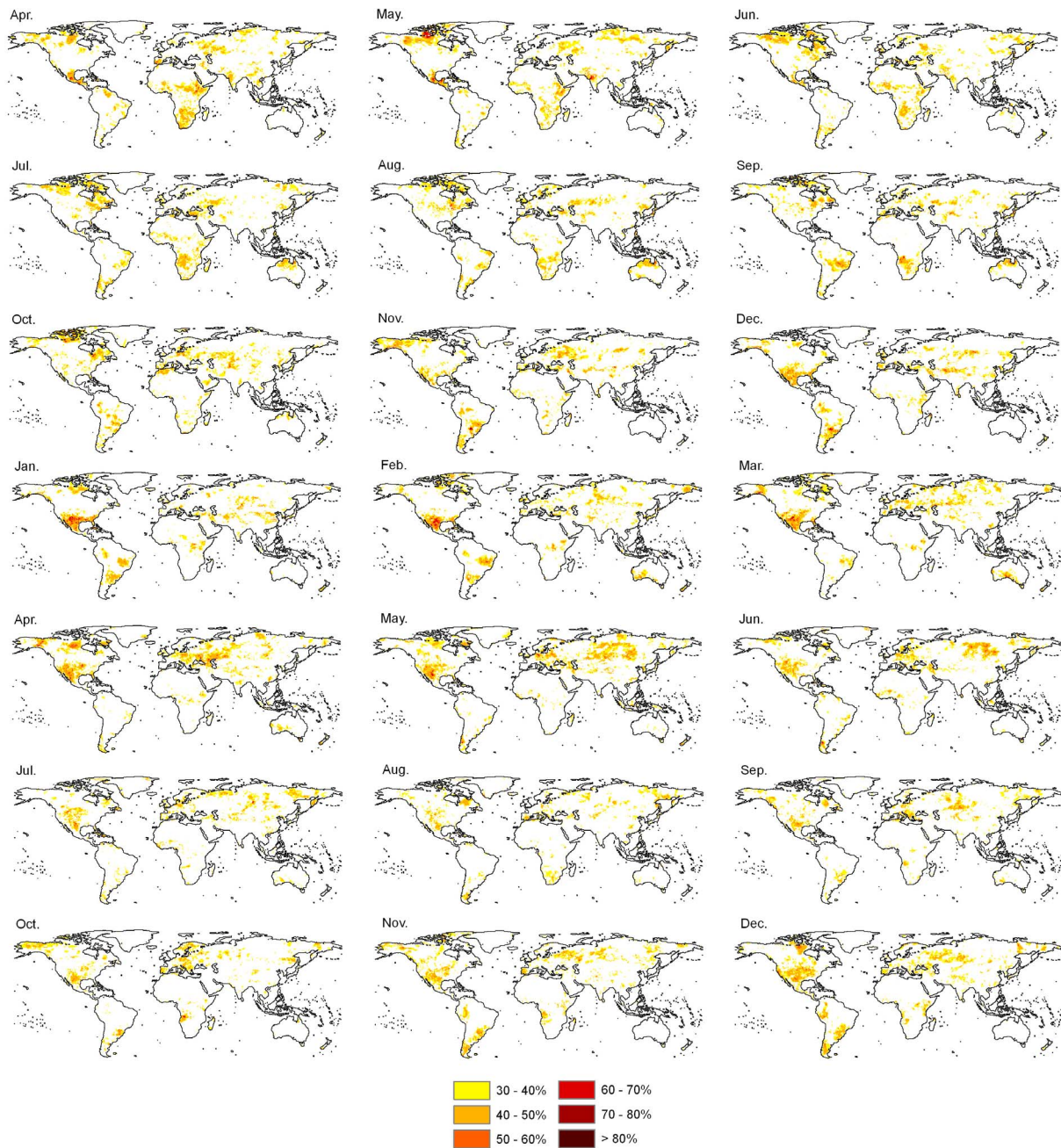


Figure 6. Probability of drought conditions (SPEI <-0.84) during La Niña events for the 3-month SPEI.

northern Mexico region, where the negative anomalies were identified from May of La Niña years and propagated to the end of the year. Other areas of the world also showed negative anomalies in some months (mainly in South America and some regions of east Africa). Nevertheless, the surface area affected was much smaller than in the Russia/Kazakhstan and USA/Mexico regions noted above.

[24] Figures 6 and 7 show the spatial distribution of the empirical probability of having drought conditions (SPEI <-0.84 , a value that represents the 20% according to the normal distribution of the SPEI values) during the year of La Niña events at the time scales of 3 and 12 months. At the time-scale of 12 months, with the exception of the southern

USA/northern Mexico region, where high probabilities were recorded for most months ($>60\%$ of La Niña years having drought conditions from July to December), the probabilities elsewhere in the world were low (commonly $<40\%$), and the spatial pattern was exceedingly patchy, even in eastern Europe and southwestern Russia.

3.2. El Niño Events and Multiscalar Droughts Globally

[25] Figure 8 shows the 1-month negative SPEI anomalies corresponding to El Niño events and the preceding year. The surface extent and duration of the anomalies show that large areas of the world had negative anomalies lasting several months. At the time scale of 1 month the impacts were

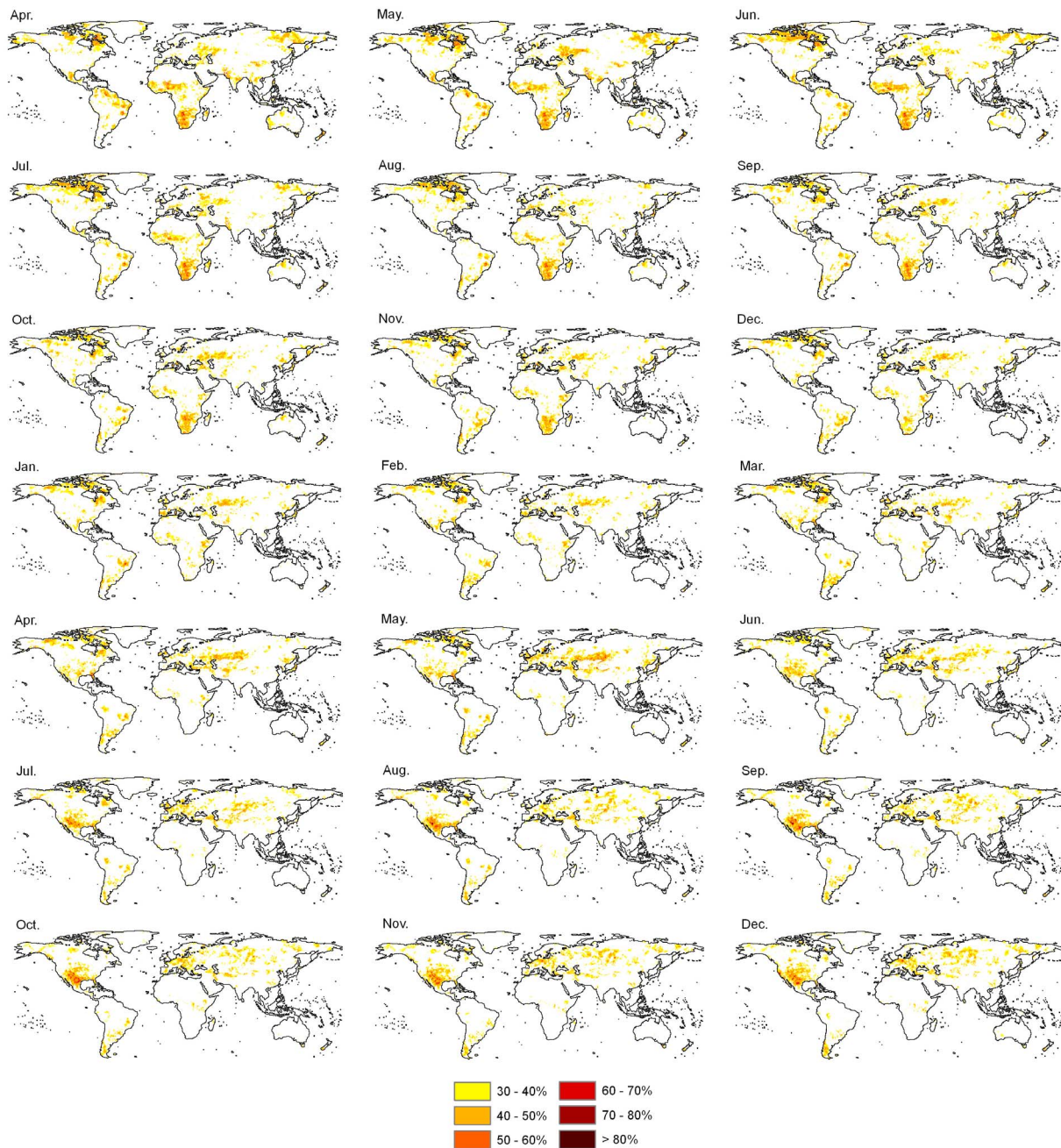


Figure 7. Probability of drought conditions (SPEI ≤ -0.84) during La Niña events for the 12-month SPEI.

evident very early in some areas. For example, the El Niño phenomenon began to cause significant negative SPEI anomalies throughout most of Australia in April of the preceding year. Three months later (in July) the anomalies affected most of Indonesia, the Indochina Peninsula, parts of India, the majority of central America, and regions of South America. The same pattern was evident between September and October, but from November of the previous year to July of the El Niño year, large areas of the world showed negative SPEI anomalies. There was substantial variability across the world with respect to the start and duration of droughts related to El Niño events. For example, generalized

negative anomalies in Australia ceased in December of the year prior to El Niño events, whereas a large area in the north of South America showed negative average anomalies from December to March; following this the negative anomalies were displaced over the Amazon and northeast Brazil, with significant impacts on drought until August. In India the negative anomalies expanded from January to June, with some major differences among months. South Africa, Canada and the Sahel region also showed negative anomalies for several months from December of the previous year to September of the El Niño year.

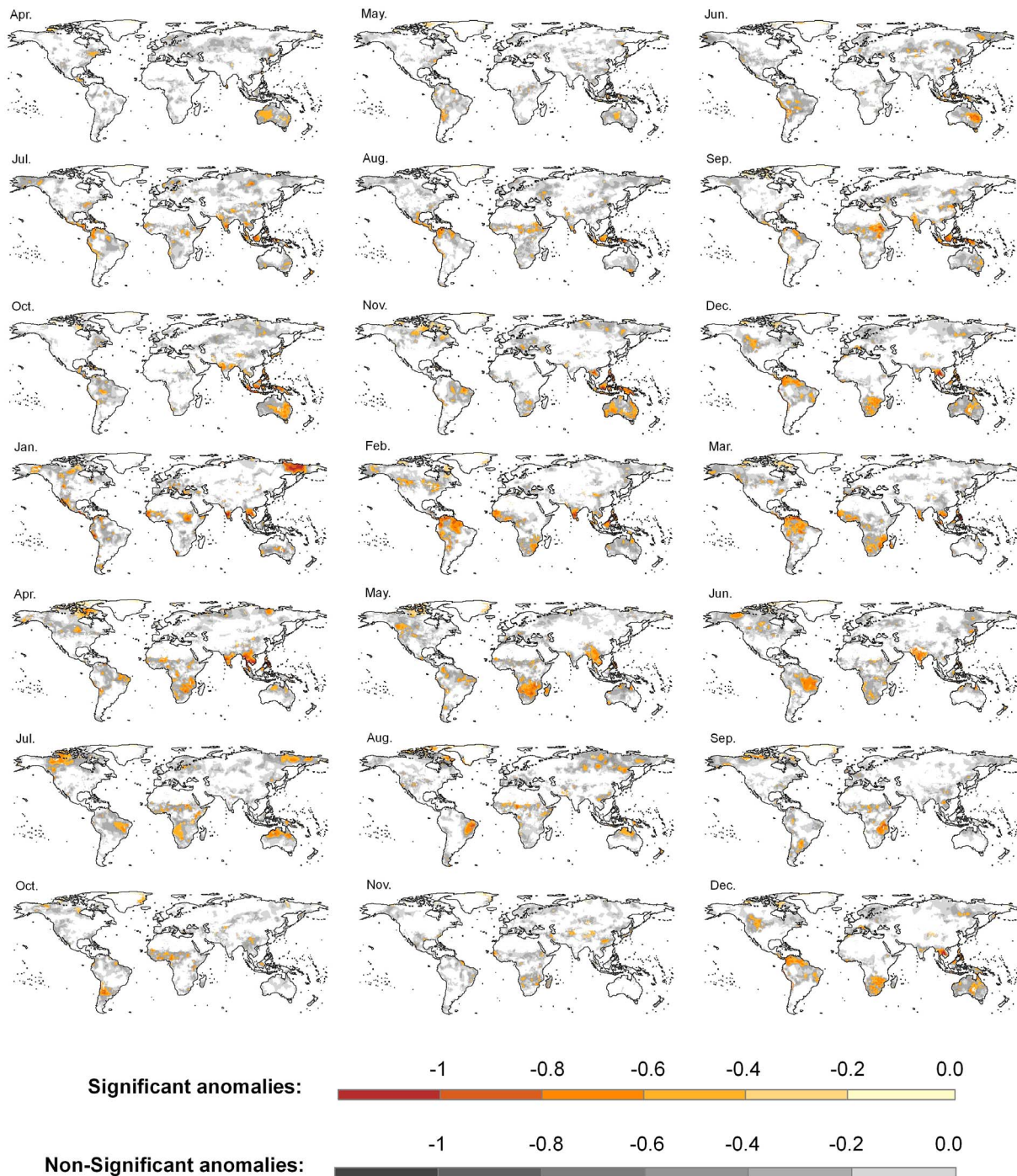


Figure 8. Spatial distribution of the average 1-month SPEI composite anomalies during El Niño years and the years preceding. Orange/reds identify areas in which significant differences in the SPEI average were found between the El Niño years and other years. Greys identify negative but non-significant anomalies.

[26] At the time scale of 3 months the spatial pattern of the negative SPEI anomalies was more homogeneous than that observed at the 1-month time scale (Figure 9). In Australia, generalized negative anomalies occurred from May of the year prior to the El Niño year to January of the El Niño year. Thus, the earliest impacts of El Niño events on droughts were evident in this region of the world. Similarly, in

Central America strong negative 3-month SPEI averages were evident from July to October in the year prior to El Niño events. The early influence of El Niño on the occurrence of dry conditions was also apparent in Indonesia. In this area significant negative SPEI anomalies lasted until March of the El Niño years. It is notable that the cumulative properties of the SPEI allow identification of the spatial

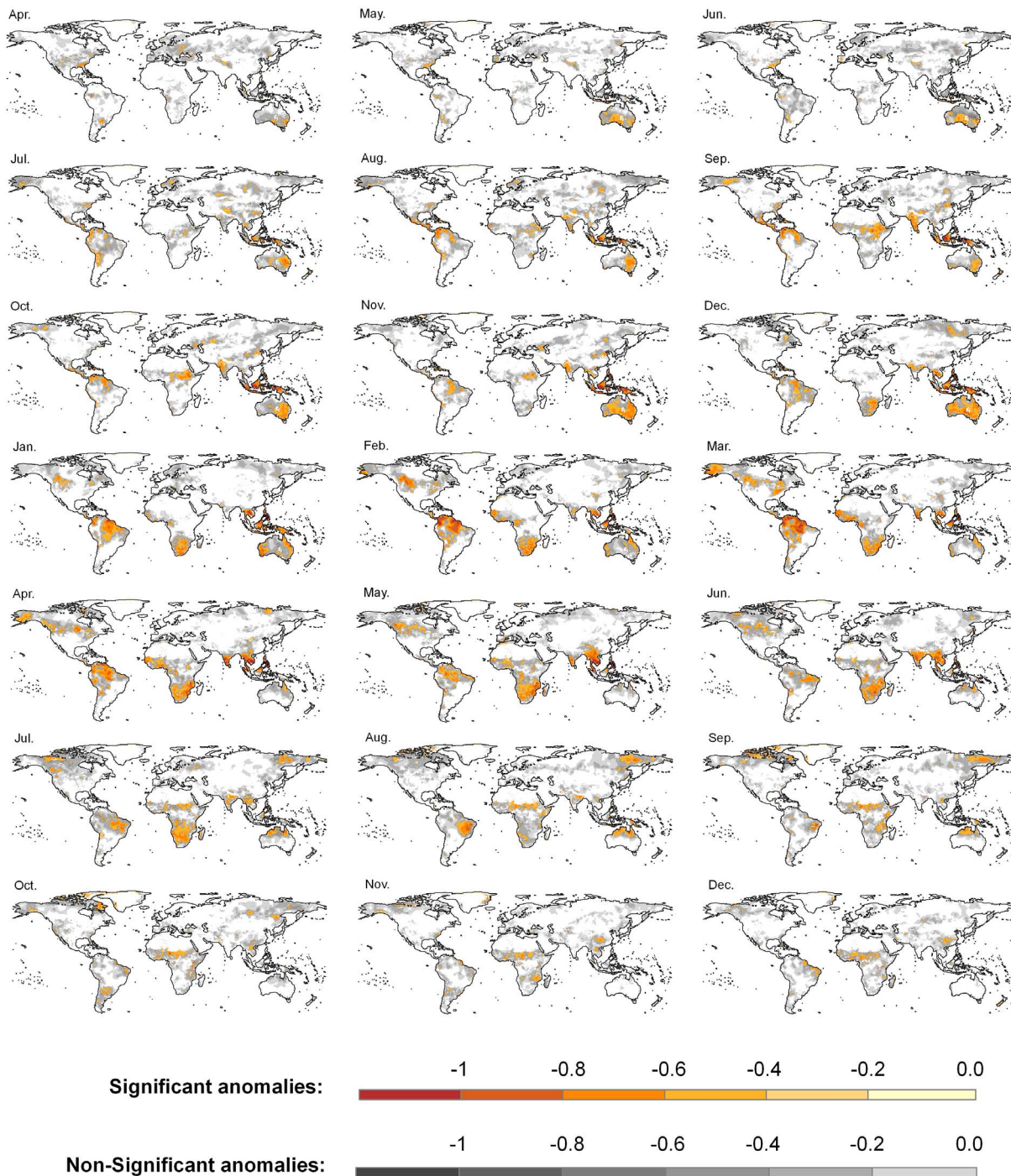


Figure 9. Spatial distribution of the average 3-month SPEI composite anomalies during El Niño years and the years preceding. Orange/reds identify areas in which significant differences in the SPEI average were found between the El Niño years and other years. Greys identify negative but non-significant anomalies.

displacements of negative SPEI anomalies among regions. For example, in the western Pacific and Indian Ocean regions it was observed that dry conditions appeared in eastern Australia very early (in April of the year prior to El Niño events), and progressively affected more areas in May and June, which are the months in which the negative anomalies moved to New Guinea. From July to November

of the year prior to El Niño events the strongest negative anomalies occurred in Indonesia, although some areas of India, Indochina and Australia were also affected. However, from January to June in El Niño years the negative anomalies were not evident in Australia and progressively disappeared from Indonesia, but Indochina and most of India were affected by very strong negative anomalies. In

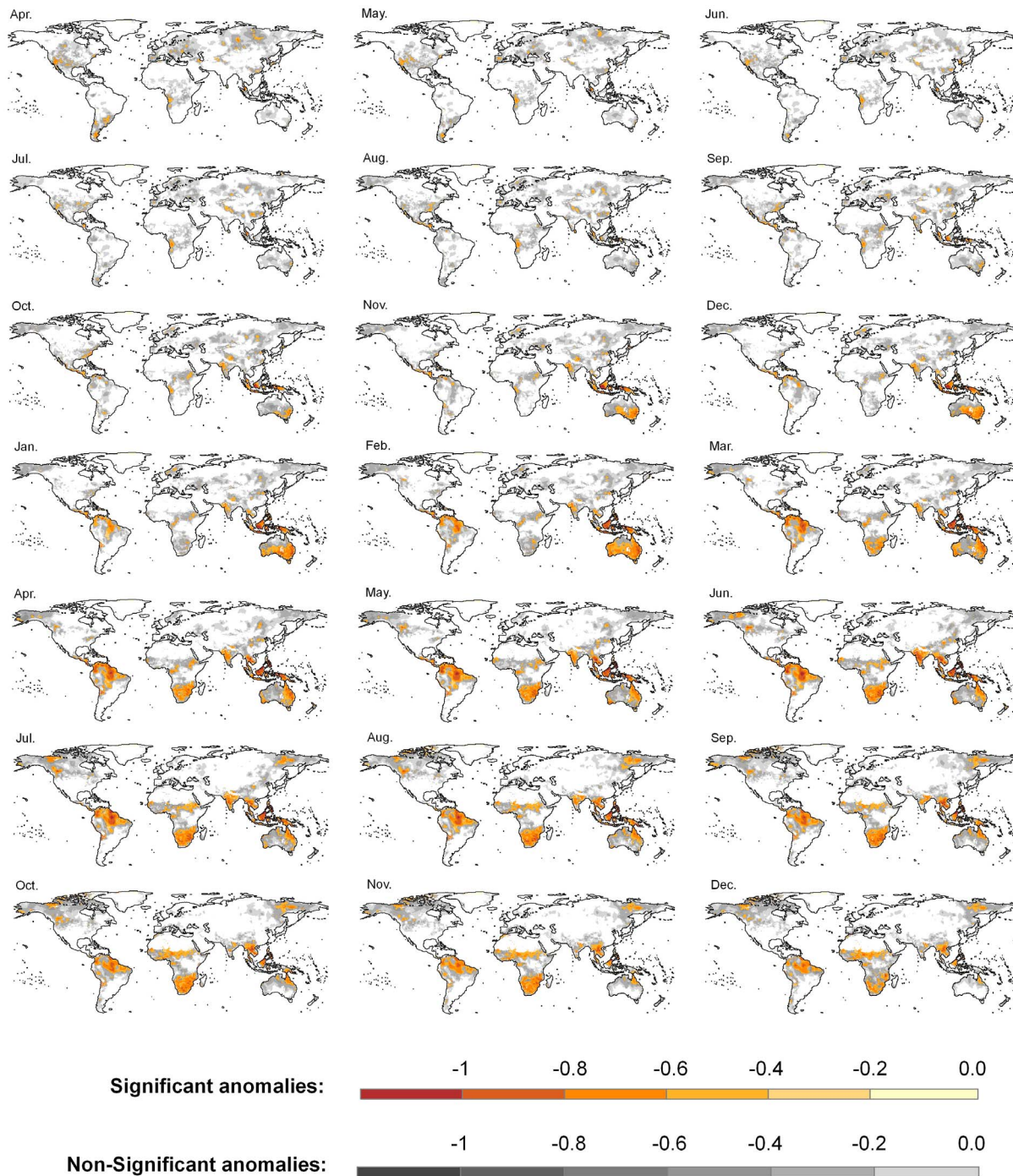


Figure 10. Spatial distribution of the average 12-month SPEI composite anomalies during El Niño years and the years preceding. Orange/reds identify areas in which significant differences in the SPEI average were found between the El Niño years and other years. Greys identify negative but non-significant anomalies.

South America the impact of El Niño events on 3-month droughts was initially evident in the northernmost region from October of the year prior to El Niño events, but strong negative anomalies affecting large areas were identified from January to April of El Niño years; the anomalies subsequently moved toward the Amazon region from May to August. Also notable were the strong negative anomalies found in large areas of Canada from January to June, the

very strong negative and generalized 3-month SPEI anomalies in the South Africa region from February to July, and the late impacts in the Sahel, from July to December.

[27] It is at the time scale of 12 months where the negative SPEI anomalies reinforce the results identified at the time scale of months; clearly the effects were delayed in time (Figure 10). Dry conditions were recorded in the western Pacific and Indian Ocean regions from September of the year

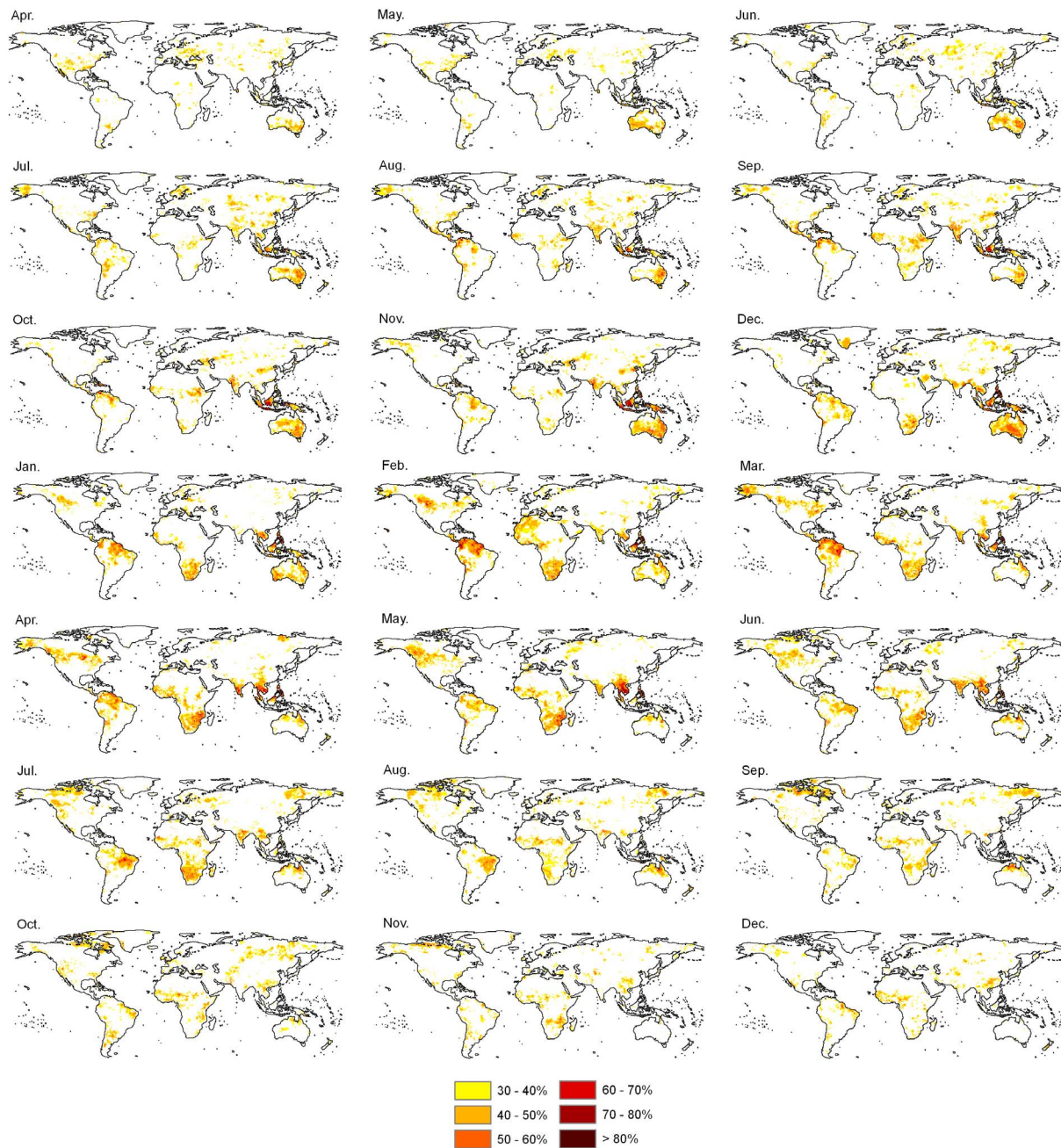


Figure 11. Probability of drought conditions (SPEI ≤ -0.84) during El Niño events for the 3-month SPEI.

prior to El Niño events to November in the El Niño year (with some spatial differences among months), but in general more homogeneous patterns were found than occurred at shorter time scales. The same pattern was observed in South America and South Africa, where the spatial patterns were more homogeneous and stable over time than those observed at shorter time scales. In contrast, other regions (e.g., Canada) where large areas were affected by negative SPEI anomalies at short time scales did not show significant negative anomalies at the time scale of 12 months.

[28] Figures 11 and 12 show the probability of having drought conditions (SPEI ≤ -0.84) at the time scales of 3 and

12 months for El Niño years. At the time-scale of 12 months the probability is very high ($>60\%$) in most of Australia and Indonesia at the beginning of the year, and in India and Indochina during the entire year. In South Africa the probability is also high ($>50\%$) during most of the months showing a very homogeneous spatial pattern in drought probability. Northern South America has the highest probability, with $>80\%$ of El Niño years associated with drought conditions. Other areas with high probabilities of drought associated with El Niño events include the Sahel, western Canada and eastern Siberia, but the surface areas affected are smaller or very patchy.

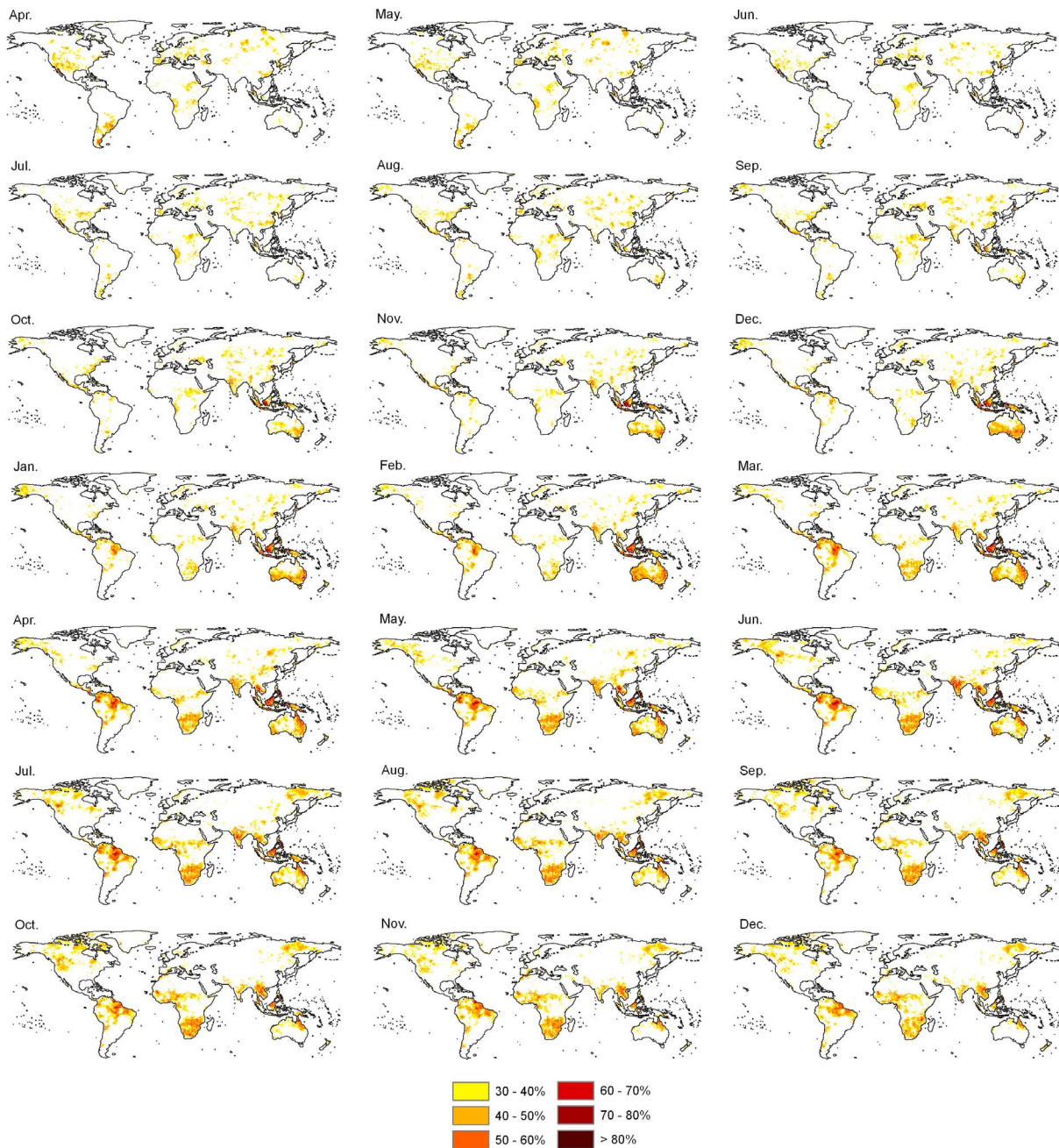


Figure 12. Probability of drought conditions (SPEI <math><-0.84</math>) during El Niño events for the 12-month SPEI.

3.3. Synthetic Analysis

[29] The figures described above identify regions of the world and the months and time scales of drought in which dry conditions are associated with extreme ENSO events (El Niño and La Niña). Figure 13 indicates the regions of the world most affected by the negative anomalies of the SPEI. As the spatial patterns of drought-affected regions commonly change among months, it is difficult to define homogeneous regions for assessing the impact. For this reason, the figure shows the average SPEI anomalies of representative locations in regions where El Niño or La Niña

events determining drought conditions were observed over a number of months and time scales. For La Niña events the regions involved were northern Mexico and southern Russia, and for El Niño events the regions involved were South Africa, Indonesia, eastern Australia, northern Brazil, India and the Sahel. In general, the regions showed how the drought conditions are recorded from short to long time-scales for the corresponding ENSO event, being more evident the effects with longer time-scales. The negative anomalies were initially recorded at short time scales during the late summer or autumn of the year prior to the event; exceptions included in eastern Australia, where anomalies

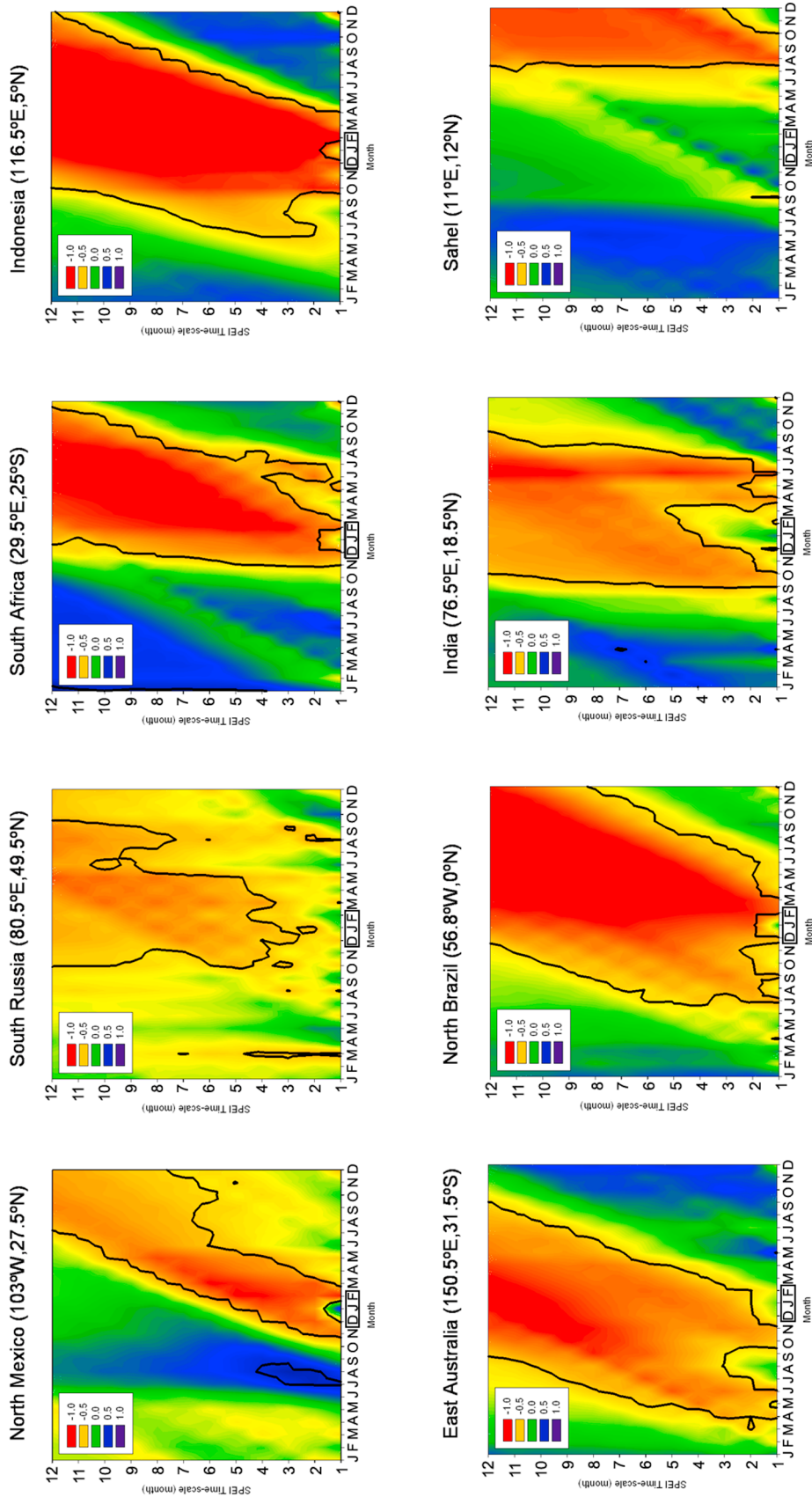


Figure 13. Average SPEI values at the time scales of 1–12 months in eight representative regions of the world during the ENSO phases that drive drought conditions in each region: i) La Niña (northern Mexico and southern Russia), and ii) El Niño (South Africa, Indonesia, eastern Australia, northern Brazil, India and the Sahel). The black lines identify months and time scales when significant differences in the SPEI averages were found between the corresponding ENSO phase and the remaining years.

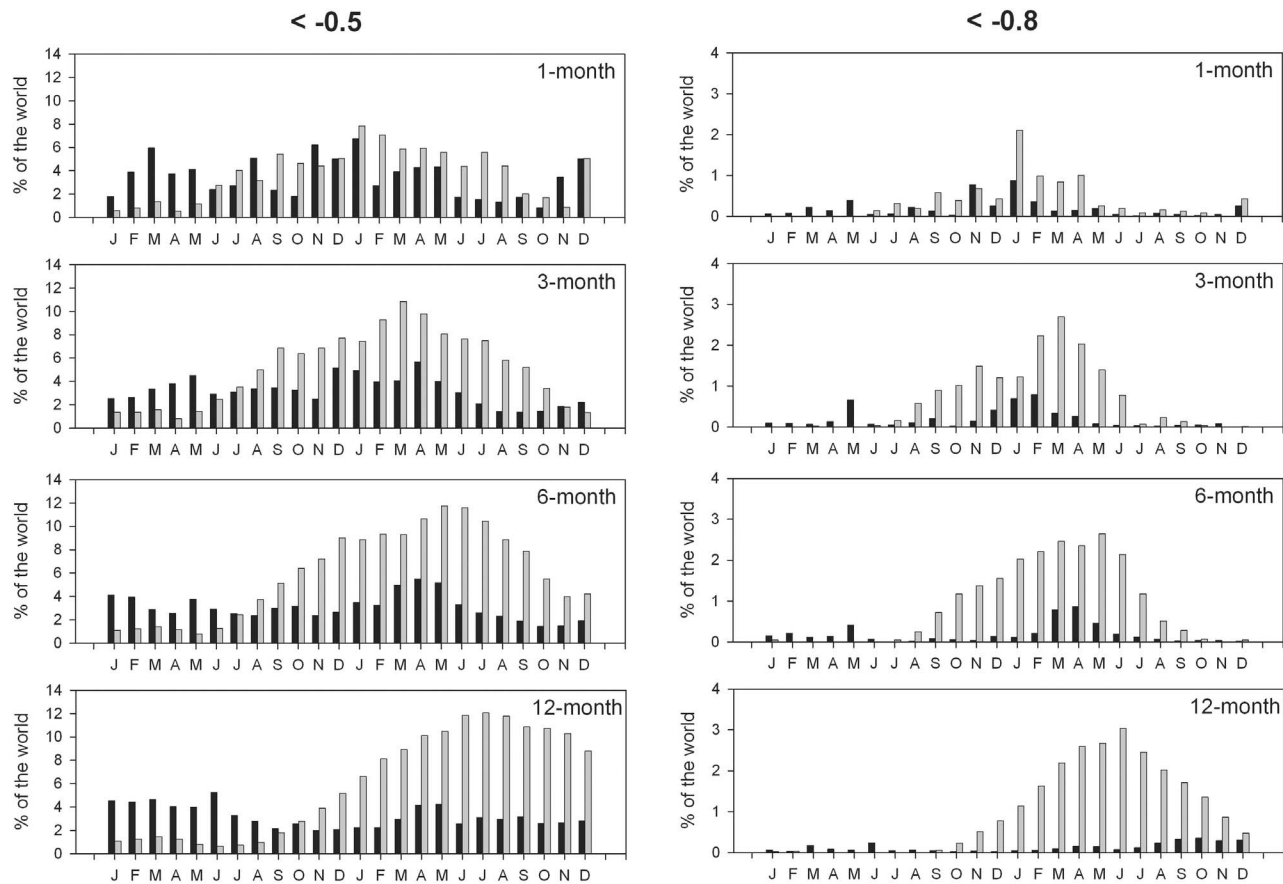


Figure 14. Percentage of the world surface where the average 1-, 3-, 6- and 12-month SPEI values were <-0.5 and <-0.8 for La Niña (black bars) and El Niño (gray bars) years and the year preceding each.

were recorded in the spring of the year preceding the event, and in the Sahel, where anomalies were recorded in summer of the preceding year. During the following months the anomalies on longer time scales strengthened as a consequence of the accumulation of the short-term negative anomalies. When the 1-month negative anomalies were recorded for different months the negative anomalies for the following months were evident at both long and short SPEI time scales (e.g., Indonesia). In contrast, when the 1-month anomalies were recorded over several months the negative anomalies were only propagated at the longer time scales. This was evident in northern Mexico, where negative anomalies at the 1-month time scale were initially evident in November of the year prior to the La Niña event, whereas two months later (in January) the 5-month time scale was the shortest for which a significant negative anomaly was found.

[30] Figure 13 shows that in regions affected by dry conditions during La Niña years (northern Mexico and southern Russia) the period with negative anomalies was shorter and of lower magnitude than occurred in regions affected by El Niño. The SPEI anomalies in South Africa, eastern Australia and northern Brazil showed very strong negative magnitudes (<-1.25) over several months in the El Niño year and in the preceding year, and encompassed various time scales. In contrast, in northern Mexico the minimum values of the average SPEI were recorded at the

6-month time scale in the year of La Niña event (SPEI = -0.95), and in southern Russia the minimum value (-0.81) was recorded in May at the 12-month time scale.

[31] Figure 14 shows the percentage of the world where the average of the 1-, 3-, 6- and 12-month SPEI values were <-0.5 and <-0.8 for La Niña and El Niño events and the preceding years. Two thresholds were selected to assess the effect on moderate and more severe global dry conditions. At the time scale of 1 month the surface of the world with average SPEI values <-0.5 oscillated about 5% for both El Niño and La Niña phases, although it was observed that for most months of the years in which the events occurred (from January to August) the surface area corresponding to El Niño phases was much greater than for La Niña phases. The difference was more evident for the surface area with SPEI values <-0.8 (corresponding to very dry conditions); the surface area affected by anomalies below this threshold was lower, but the difference between the El Niño and La Niña events was much clearer. The differences between El Niño and La Niña phases at the time scale of 1 month were magnified at longer time scales. At the time scale of 3 months more than the 6% of the world showed average SPEI values <-0.5 from September of the year prior to El Niño phases to October of the El Niño year, but for late spring and early summer (April to July) 10% of the world showed an average SPEI <-0.5 . In contrast, during La Niña phases the surface area affected by droughts was much

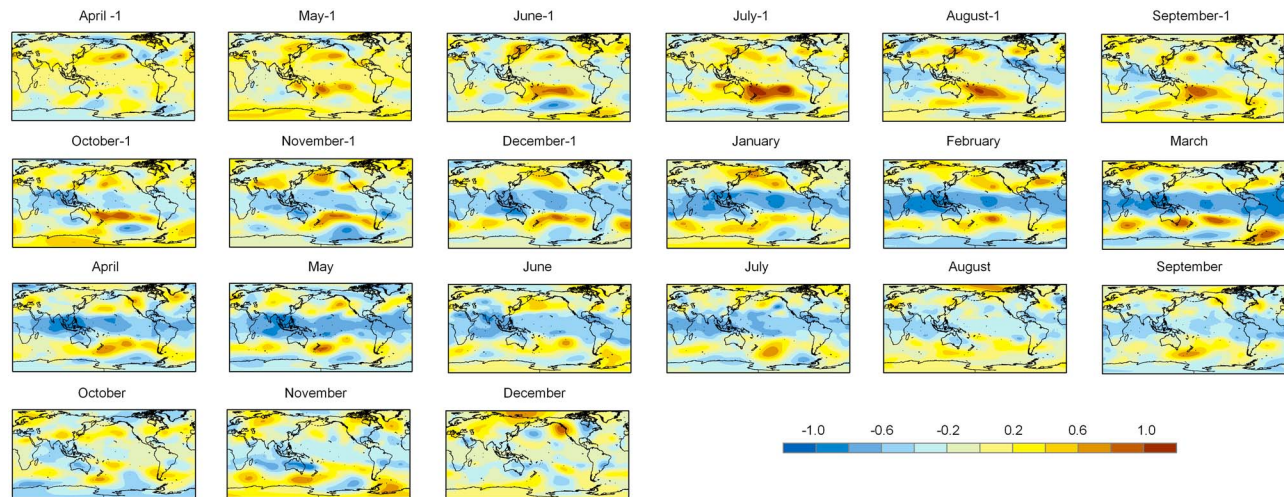


Figure 15. The 500 hPa standardized anomalies during La Niña years and the years preceding.

lower (<5%). The difference was even more evident for an SPEI threshold of -0.8 , because very few areas of the world were identified with La Niña phases compared with 2–3% of the world with El Niño phases. The differences were enhanced at time scales of 6 and 12 months, especially for the most severe droughts ($\text{SPEI} < 0.8$).

3.4. Related Atmospheric Mechanisms

[32] Figure 15 shows the average values of the standardized 500 hPa geopotential heights corresponding to La Niña years. Large negative 500 hPa geopotential heights anomalies are recorded in the Pacific region, but also propagated throughout the intertropical zone around the globe, from November of the previous year to July of La Niña year. This could be explained further by the observed cooling of the Eastern Pacific basin, as it is shown with the large negative SST anomalies identified over most of this tropical region from August of the preceding year to May of La Niña year (see Figure S3 in the auxiliary material Text S1).¹ In addition, there are moderate positive 500 hPa geopotential heights anomalies affecting the southern and western part of North America during the months in which the most negative SPEIs at the time scale of 1 month were recorded in this region (November, December, February and March) (see Figure 3). Also in the Eastern Europe, the pattern of dominant negative 1-month SPEI is related to positive pressure 500 hPa anomalies, light to moderate from February to May during La Niña year. The surface conditions represented by the Sea Level Pressure (SLP) anomalies could also help to explain the pattern of negative SPEI anomalies observed during La Niña phases over these regions (see Figure S4 in the auxiliary material Text S1). In any case, the magnitude of the 500 hPa geopotential heights and SLP anomalies and the general atmospheric circulations prone to cause droughts are progressively smoothed from May of La Niña year. This would explain

the very few negative SPEI anomalies at the time scale of one month recorded from May of La Niña year worldwide.

[33] During El Niño episodes, strong positive SST anomalies in the Eastern Pacific basin are observed from June of the previous year to May of the El Niño year (see Figure S5 in the auxiliary material Text S1). These large positive SST anomalies dramatically affect the low- and mid-level atmospheric circulation during several months. In the case of El Niño, it is very clear that the effect on the 1-month negative SPEI anomalies is driven by different factors as a function of the region of the world. The early effects of the El Niño are recorded in Indonesia (from July to December of the previous year; see Figure 8) and Australia (mainly from October to December of the previous year; see Figure 8), and they are mainly driven by the strong positive SLP anomalies observed over the Western Pacific basin (Figure 16). The colder than average SSTs in the Western Pacific region are having a clear effect on the SLP conditions, resulting in a strong anticyclonic weather pattern centered over Indonesia. This is a simultaneous effect of the El Niño on the drought conditions driven by coupled sea surface–low troposphere interactions. Nevertheless, the main effects of El Niño on droughts are propagated by means of the mid-troposphere anomalies summarized by the maps of anomalies at the 500 hPa geopotential height (see Figure 17). High pressure SLP anomalies in the Western Pacific basin between September of the previous year to April of El Niño year propagates to the mid-level troposphere between November of the previous year to June of El Niño year (particularly stronger in February–March), determining the occurrence of strong high pressure anomalies at the 500 hPa level in most of the intertropical area. Therefore, there is a clear propagation of the negative SST anomalies to the positive SLP anomalies observed in the Western Pacific basin. Consequently, these low-level anomalies are propagated throughout the entire intertropical region reinforcing anticyclonic conditions at mid-level of the troposphere 6 months after the SST anomalies in the Western Pacific region develop. Whereas for La Niña years very few land areas are affected by positive 500 hPa

¹Auxiliary materials are available in the HTML. doi:10.1029/2011JD016039.

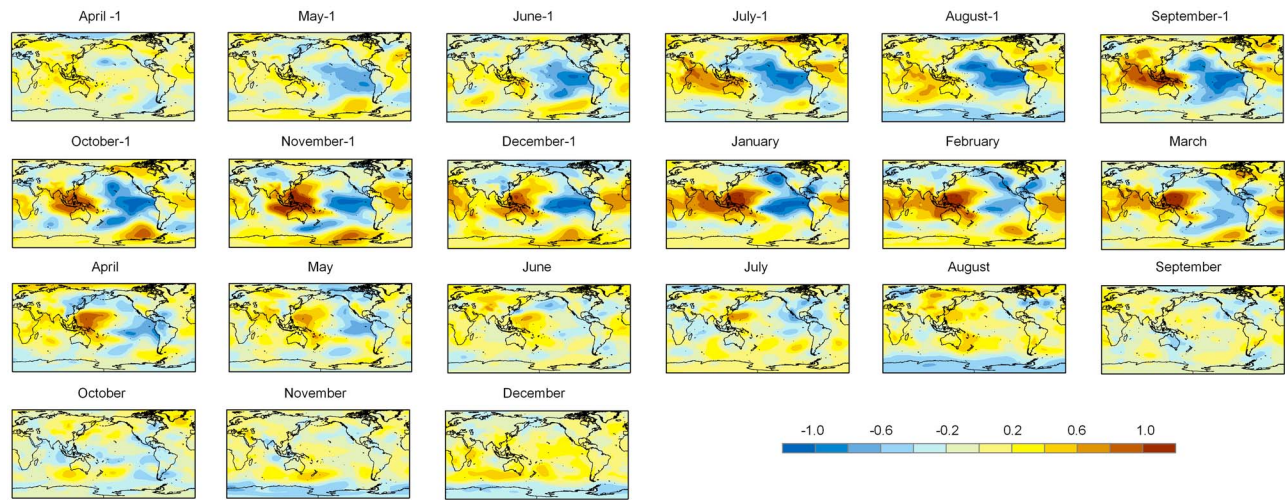


Figure 16. SLP standardized anomalies during El Niño years and the years preceding.

geopotential height anomalies, for El Niño years a large emerged area shows a dominant anticyclonic circulation. For example, in the case of Australia and Indochina the first strong positive 500 hPa anomalies are recorded in November and December of the previous year, corresponding to strong negative 1-month SPEI anomalies over most of the region. Thus, there is a high agreement between the areas with the strongest positive anomalies in surface and 500 hPa pressures and the most negative SPEIs recorded each month of El Niño phase. For instance, the negative 1-month SPEIs are recorded in Canada, northern part of South America, South Africa, South India, and the Asian region from Indochina to the North Australia in December of the previous year, which correspond to the regions with the strongest positive anomalies at the 500 hPa geopotential height. From January to July of the El Niño year, negative 1-month SPEI values are recorded in different regions of the world affected by positive pressure anomalies at the mid-troposphere, which are very persistent in areas like South Africa and South India where the negative 1-month

SPEI values are recorded in most of the months from February to July of El Niño year.

[34] The results show that although the patterns of anomalies of SST, SLP and 500 hPa heights are persistent for different months of El Niño and La Niña phases, the influence on the areas in which the ENSO phenomenon is determining drought conditions is restricted to few months at the time scale of 1 month. Therefore, the delays in the drought onset at longer time scales (e.g., 6- or 12-months) occur due to a delay in the local hydrological response and are not associated with the atmospheric circulation response to the SST anomalies or the evolution of the SST anomaly itself. As a result, the anomalies recorded at longer time-scales, representative of different types of drought, will be caused by the cumulative dry conditions in some specific months, commonly coeval with the strongest ENSO signal in the SST and atmospheric circulation anomalies. These anomalies will then propagate throughout the hydrological cycle to cause droughts at long time-scales. Nevertheless, for El Niño phases, the persistence of the 1-month SPEI

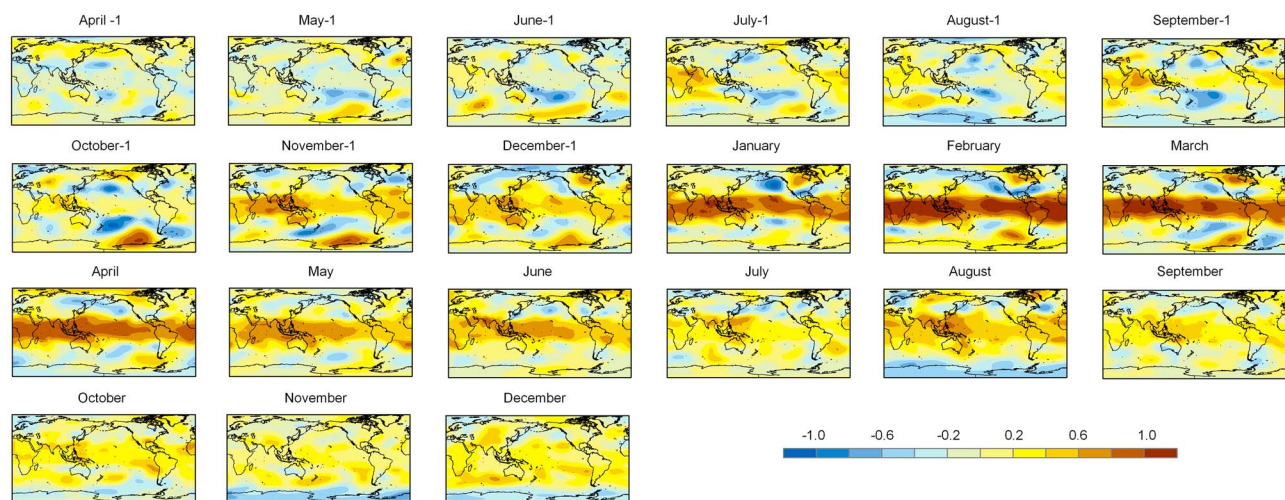


Figure 17. The 500 hPa standardized anomalies during El Niño years and the years preceding.

anomalies is commonly stronger than that found for La Niña phases (e.g., in the northern South America and South Africa), explaining that droughts are propagated at longer SPEI time-scales several months after finishing the SST and related atmospheric circulation anomalies.

4. Discussion and Conclusions

[35] We presented here the first global analysis of the ENSO impact on multiscalar droughts, focusing on the effects of the warm (El Niño) and cold (La Niña) events of the ENSO phenomenon. The results showed that very dry conditions occurred during both phases in different areas of the world. Thus, the spatial extent and the months in which the impacts were recorded varied significantly during the events. Although our results are consistent in general terms with previous findings at global [e.g., Kousky *et al.*, 1984; Ropelewski and Halpert, 1987, 1996; Halpert and Ropelewski, 1992; Kiladis and Diaz, 1989; Diaz *et al.*, 2001; Dai *et al.*, 2004; Sheffield *et al.*, 2009; Apipattanasri *et al.*, 2009] and regional scales [e.g., Harger, 1995; Chiew *et al.*, 1998; Bonsal and Lawford, 1999; Richard *et al.*, 2001; Karanaskas *et al.*, 2008; Espinoza Villar *et al.*, 2009; Kothawale *et al.*, 2010], we have provided strong evidence that the magnitude of the drought conditions recorded in each region shows large variations as a function of the drought time scale. Thus, the results showed that the period in which dry conditions were identified in each affected region tended to increase by some months as the time scale became longer. This resulted from the procedure for calculation of the multiscalar drought index, because longer time scales generated smoother fluctuations and thus a larger sequence of anomalies with the same sign. The main implication of the results is the potential to improve assessment of the possible agricultural, environmental, hydrological and economic impacts, based on the ability of the different drought time scales to represent the temporal variability of various usable water sources.

[36] Nevertheless, it is noteworthy that both the timing of the impacts and the spatial pattern of negative SPEI anomalies for both the warm and cold phases varied as a function of the time scale. At short time scales the main regions affected by negative SPEI anomalies were clearly identified. However, they showed some variability, with large differences in the spatial patterns and the magnitude of the anomalies among the months of the event. Thus, at short time scales the negative anomalies that were identified showed a very patchy pattern, which was more evident during La Niña events. In contrast, at longer time scales the spatial pattern of negative anomalies was more coherent; fewer but larger regions were affected, and the temporal variability in the affected areas and the magnitude of the anomalies was low. Thus, longer time scales emphasized the ENSO effects and clearly distinguished regions where the expected influence of the ENSO phases was uncertain or statistically significant. At short time scales sustained negative anomalies during most ENSO phases will produce marked dry conditions at longer time scales. In contrast, the influence on droughts is smoothed at longer time scales in those regions only affected over a few months, or where the events exhibit negative anomalies. As mentioned above, this will have significant consequences for those hydrological

subsystems with long response times to dry climate conditions, such as groundwater reserves and large reservoirs [e.g., Peters *et al.*, 2005; Lorenzo-Lacruz *et al.*, 2010].

[37] This study highlighted a number of regions that are markedly affected by drought at a wide range of time scales in response to El Niño and La Niña phases. Those regions affected by La Niña phases were southern USA/northern Mexico and southern Russia/eastern Europe, whereas for El Niño phases the most affected areas were South Africa, Indonesia and the western Pacific area, Australia, the northern part of South America and the Amazon, India and the Indochina peninsulas, central and western Canada, and large areas of the Sahel. These results agree with the impact of positive and negative ENSO phases on global precipitation. For example, Ropelewski and Halpert [1987] showed in the West Pacific region and El Niño phases low precipitation during most of the months of the year. In India the negative precipitation anomalies are found between June and September of the previous year to El Niño and in South Africa between July of the previous year and March of El Niño years, a similar pattern that found in northeastern South America. Thus, we found negative SPEI anomalies for most of these months and regions by means of a SPEI 1-month time-scale. Ropelewski and Halpert [1989] also analyzed La Niña phases, showing a smaller number of anomalies associated with La Niña phases in relation to those identified for El Niño. Nevertheless, these previous global studies showed lower precipitation anomalies for La Niña phases than the drought anomalies identified here (e.g., South North America). The droughts associated with La Niña phases in Southern USA and Northern Mexico were described by Kahya and Dracup [1994], which detected negative streamflow anomalies appearing at the beginning of La Niña event year until October of the same year. In any case, at the time-scale of 1 month the magnitude of the negative SPEI anomalies found worldwide are, in general, low and comparable to the magnitude observed by the studies cited above using monthly precipitation. Thus, we clearly observe that when the cumulative effects summarized by longer SPEI time-scales are analyzed larger anomalies are identified.

[38] We have also analyzed the Sea Surface Temperature and the atmospheric circulation patterns that the ENSO signal propagates on droughts worldwide. Although the dynamic of the El Niño and La Niña phases had been widely analyzed [e.g., Rasmusson and Carpenter, 1982; Clarke, 2008, and references therein] and also their connection with the surface climate [e.g., Gershunov and Barnett, 1998; Allan *et al.*, 1996], we have illustrated here the high relationship between atmospheric circulation anomalies and the SPEI averages in those regions in which El Niño or La Niña phases are prone to cause droughts. The effect of the ENSO phases on droughts is mainly propagated throughout the mid-troposphere [Enfield and Mestas-Núñez, 1999; Mo, 2000], with a delay of some months regarding the SLP anomalies in the Western Pacific area as a consequence of the colder than average SST anomalies. The effect of the anomalies in the atmospheric circulation on dry conditions are detected for several months of each one of the ENSO phases, but mainly for El Niño years in which persistent negative SPEIs at the time scale of 1-month are recorded in some regions (e.g., South Africa or India). Nevertheless, the

drought conditions at longer time-scales (e.g., 6- or 12-months) are not directly determined by the atmospheric circulation response to the SST anomalies, since the SPEI anomalies will be caused by a persistence of the drought signal even when the precipitation conditions go back to normality, as it takes time to build up the regional available water back to a normal level even after precipitation is back to normal.

[39] The number of regions and months affected and the total surface area with negative anomalies was much higher for El Niño events than for La Niña events. In summary, El Niño events tended to generate more droughts globally than La Niña events. This is in agreement with the recent findings of *Sheffield et al.* [2009], who showed that there is a tendency for more short-term drought events to occur during El Niño phases. Nevertheless, our results show that the tendency to more regions and stronger negative anomalies for El Niño events relative to La Niña events clearly increases with an increase in the time scale over which the drought is quantified. Thus, at the longest time scales the percentage of the global surface area affected by drought during El Niño years was more than four times that for La Niña years. This implies that El Niño events affect more regions and have greater impact, but also that the associated dry conditions are more persistent over time. *Smith and Ropelewski* [1997] concluded that (i) in several regions where the ENSO influence has been identified, the impact is greater for one phase (El Niño or La Niña) than the other, and (ii) in general, the precipitation at the global scale is greater during La Niña events than during El Niño events, which is a pattern that has also been observed for soil moisture modeled at the global scale [*Sheffield et al.*, 2009]. This result is expected because during El Niño events tropical precipitation shifts to the central Pacific Ocean and away from tropical land areas. Thus, during El Niño phases tropical landmasses dry while wet over land is restricted to southern North America and a small part of southern South America. The opposite is true during La Niña events.

[40] Our results also showed differences in the timing of the influence of ENSO events in different regions of the world, independent of the drought time scale. There is an evolution in the ENSO cycle, both the SST pattern and the atmospheric teleconnection, with some regions being affected later in the ENSO cycle relative to the peak [*Kiladis and Diaz*, 1989; *Stone et al.*, 1996]. The lags in the ENSO impact are very complex when quantified at various time scales. Nevertheless, in the most affected regions of the world we did not find early effects (at the beginning of the corresponding ENSO events) during La Niña phases, whereas for El Niño phases early effects were clearly evident in areas including Australia and Indonesia. Moreover, the effects of El Niño phases lasted for many months, and in some regions (e.g., the Sahel) the impact of El Niño on droughts could be detected more than one year after the beginning of the warm phase.

[41] It is notable that the effect of ENSO events on droughts clearly lagged in different regions of the world, and that there was spatial displacement of the affected areas to neighboring regions as the ENSO event developed: the most obvious case was the displacement of drought conditions toward Indonesia from Australia at the beginning of El

Niño events, followed by advance to the Indochina peninsula and finally to India.

[42] The sequence in the development of drought conditions around the world at various points of the ENSO cycle as the global ENSO precipitation and temperature signal develops offer a unique mechanism for drought prediction. The development of measures for drought planning and preparedness is a priority in reducing drought hazards [*Wilhite*, 1996; *Wilhite et al.*, 2007; *Prabhakar and Shaw*, 2008]. A critical component in drought planning is the provision of timely and reliable climate information on which to base management decisions [*Svoboda et al.*, 2004]. Hence, drought monitoring is crucial for the implementation of drought plans and the use of synthetic drought indicators, including the SPEI used in this study. Such indicators can provide quantitative information about the spatial extent and severity of drought conditions in a way that reflects the level of risk in real time.

[43] The capacity to accurately predict droughts prior to their onset would markedly improve the management of risk, and reduce its associated impacts. However, relative to drought monitoring the forecasting of droughts is still unreliable. Objective methodologies to forecast droughts based on systems including climate, land surface and hydrologic models are under experimentation, but although drought prediction is a complex emerging effort, in the USA operative droughts forecasting is based on a combination of sources including the Constructed Analogue on Soil moisture, the Climate Forecast System seasonal precipitation forecasts, normal climatology and the El Niño precipitation and temperature composites for November–January (see details provided by *Schubert et al.* [2007]). Recent studies in Europe have indicated the possibility of providing seasonal anomaly forecasts, using the influence of driving factors including the ENSO phase [*Friás et al.*, 2010].

[44] The prediction of ENSO events has increased with the refinement of numerical models [*Chen et al.*, 2004; *Tippett and Barnston*, 2008; *Jin et al.*, 2008]. However, we have shown that prediction of drought impacts related to ENSO can be possible too based only on observations, because there is commonly a delay of some months from the onset of ENSO events (typically in April–May of the previous year) to the occurrence of drought. The prediction can be even more robust for those water sources related to long drought time scales (e.g., groundwater and reservoir storages), where the delay is even longer. In regions such as Australia, where the ENSO impact on droughts are identified very early (at the beginning of the ENSO phases), the potential to predict is very limited and dependent on numerical prediction of the occurrence of ENSO events. Given the large temporal lag between the development of ENSO phenomena and the identification of drought conditions, it appears possible to detect in advance the likely impact of the ENSO on drought in the majority of regions, at time scales comparable to those in this study. Nevertheless, although useful, we must also be aware that composite analyses and statistical methodologies like the one presented here cannot capture the evolution of non-typical ENSO events and long-term stationarities in the global ENSO teleconnections. This can only be achieved by improved dynamical predictions based on climate models, which have showed a high reliability to detect the ENSO impacts

throughout the world [Roeckner et al., 1996; Achuta Rao and Sperber, 2002; Wu and Kirman, 2006].

[45] Although some studies have found a nonstationary relationship between the surface climate and the ENSO variability in some regions [e.g., Lloyd-Hughes and Saunders, 2002; Kane, 2006], recent analyses have demonstrated that the linear ENSO teleconnections are stable and robust, and there is no evidence that changes in the strength of the teleconnections between ENSO and the atmospheric circulation went beyond chance in the recent past [Sterl et al., 2007]. Established relationships between ENSO phases and drought indices therefore seem appropriate for drought prediction over large areas of the world.

[46] **Acknowledgments.** This work has been supported by the research projects CGL2006-11619/HID, CGL2008-01189/BTE, CGL2011-27574-CO2-02, CGL2011-27753-CO2-01 and CGL2011-27536 financed by the Spanish Commission of Science and Technology and FEDER, EUROGEOS (FP7-ENV-2008-1-226487) and ACQWA (FP7-ENV-2007-1- 212250) financed by the VII Framework Programme of the European Commission, “Efecto de los escenarios de cambio climático sobre la hidrología superficial y la gestión de embalses del Pirineo Aragonés” financed by “Obra Social La Caixa” and the Aragón Government and “Influencia del cambio climático en el turismo de nieve.” CTTP01/10, financed by the Comisión de Trabajo de los Pirineos.

References

- Achuta Rao, K., and K. R. Sperber (2002), Simulation of the El Niño Southern Oscillation: Results from the Coupled Model Intercomparison Project, *Clim. Dyn.*, *19*, 191–209, doi:10.1007/s00382-001-0221-9.
- Allan, R., J. Lindesay, and D. Parker (1996), *El Niño Southern Oscillation and Climatic Variability*, 416 pp., CSIRO, Clayton South, Victoria, Australia.
- Apipattanasri, S., G. J. McCabe, B. Rajagopalan, and S. Gangopadhyay (2009), Joint spatiotemporal variability of global sea surface temperatures and Global Palmer Drought Severity Index values, *J. Clim.*, *22*, 6251–6267, doi:10.1175/2009JCLI2791.1.
- Ashok, K., and T. Yamagata (2009), The El Niño with a difference, *Nature*, *461*, 481–484, doi:10.1038/461481a.
- Balling, R. C., Jr., and G. B. Goodrich (2007), Analysis of drought determinants for the Colorado River Basin, *Clim. Change*, *82*, 179–194, doi:10.1007/s10584-006-9157-8.
- Beguieria, S., S. M. Vicente-Serrano, and M. Angulo (2010), A multi-scalar global drought data set: The SPEIbase: A new gridded product for the analysis of drought variability and impacts, *Bull. Am. Meteorol. Soc.*, doi:10.1175/2010BAMS2988.1.
- Bonsal, B. R., and R. G. Lawford (1999), Teleconnections between El Niño and La Niña events and summer extended dry spells on the Canadian prairies, *Int. J. Climatol.*, *19*, 1445–1458, doi:10.1002/(SICI)1097-0088(19991115)19:13<1445::AID-JOC431>3.0.CO;2-7.
- Breshears, D. D., et al. (2005), Regional vegetation die-off in response to global-change-type drought, *Proc. Natl. Acad. Sci. U. S. A.*, *102*, 15,144–15,148, doi:10.1073/pnas.0505734102.
- Brönnimann, S. (2007), Impact of El Niño–Southern Oscillation on European climate, *Rev. Geophys.*, *45*, RG3003, doi:10.1029/2006RG000199.
- Brönnimann, S., J. Luterbacher, J. Stahelin, T. M. Svendby, G. Hansen, and T. Svenøe (2004), Extreme climate of the global troposphere and stratosphere in 1940–42 related to El Niño, *Nature*, *431*, 971–974, doi:10.1038/nature02982.
- Brown, J. N., P. C. McIntosh, M. J. Pook, and J. S. Risbey (2009), An investigation of the links between ENSO flavors and rainfall processes in Southeastern Australia, *Mon. Weather Rev.*, *137*, 3786–3795, doi:10.1175/2009MWR3066.1.
- Chen, D., M. A. Cane, A. Kaplan, S. E. Zebiak, and D. J. Huang (2004), Predictability of El Niño over the past 148 years, *Nature*, *428*, 733–736, doi:10.1038/nature02439.
- Chiew, F. H. S., T. C. Piechota, J. A. Dracup, and T. A. McMahon (1998), El Niño/Southern Oscillation and Australian rainfall, streamflow and drought: Links and potential for forecasting, *J. Hydrol.*, *204*, 138–149, doi:10.1016/S0022-1694(97)00121-2.
- Ciais, P., et al. (2005), Europe-wide reduction in primary productivity caused by the heat and drought in 2003, *Nature*, *437*, 529–533, doi:10.1038/nature03972.
- Clarke, A. (2008), *An Introduction to the Dynamics of El Niño & the Southern Oscillation*, 324 pp., Academic, San Diego, Calif.
- Compo, G. P., et al. (2011), The Twentieth Century Reanalysis Project, *Q. J. R. Meteorol. Soc.*, *137*, 1–28, doi:10.1002/qj.776.
- Cordery, I., and M. McCall (2000), A model for forecasting drought from teleconnections, *Water Resour. Res.*, *36*, 763–768, doi:10.1029/1999WR900318.
- Dai, A., K. E. Trenberth, and T. Qian (2004), A global dataset of Palmer Drought Severity Index for 1870–2002: Relationship with soil moisture and effects of surface warming, *J. Hydrometeorol.*, *5*, 1117–1130, doi:10.1175/JHM-386.1.
- D’Arrigo, R., and R. Wilson (2008), El Niño and Indian Ocean influences on Indonesian drought: Implications for forecasting rainfall and crop productivity, *Int. J. Climatol.*, *28*, 611–616, doi:10.1002/joc.1654.
- Díaz, H. F., and G. N. Kiladis (1992), Atmospheric teleconnections associated with the extreme phases of the Southern oscillation, in *El Niño: Historical and Paleoclimatic Aspects of the Southern Oscillation*, edited by H. F. Diaz and V. Markgraf, pp. 7–28, Cambridge Univ. Press, Cambridge, U. K.
- Díaz, H. F., M. P. Hoerling, and J. K. Eischeid (2001), ENSO variability, teleconnections and climate change, *Int. J. Climatol.*, *21*, 1845–1862, doi:10.1002/joc.631.
- Enfield, D. B., and A. M. Mestas-Núñez (1999), Multiscale variabilities in global sea surface temperatures and their relationships with tropospheric climate patterns, *J. Clim.*, *12*, 2719–2733, doi:10.1175/1520-0442(1999)012<2719:MVIGSS>2.0.CO;2.
- Espinoza Villar, J. C., et al. (2009), Spatio-temporal rainfall variability in the Amazon basin countries (Brazil, Peru, Bolivia, Colombia, and Ecuador), *Int. J. Climatol.*, *29*, 1574–1594, doi:10.1002/joc.1791.
- Fiorillo, F., and F. M. Guadagno (2010), Karst spring discharges analysis in relation to drought periods, using the SPI, *Water Resour. Manage.*, *24*(9), 1867–1884, doi:10.1007/s11269-009-9528-9.
- Fowler, A., and K. Adams (2004), Twentieth century droughts and wet periods in Auckland (New Zealand) and their relationship to ENSO, *Int. J. Climatol.*, *24*, 1947–1961, doi:10.1002/joc.1100.
- Frías, M. D., S. Herrera, A. S. Cofiño, and J. M. Gutiérrez (2010), Assessing the skill of precipitation and temperature seasonal forecasts in Spain: Windows of opportunity related to ENSO events, *J. Clim.*, *23*, 209–220, doi:10.1175/2009JCLI2824.1.
- Fu, C., H. F. Diaz, and J. O. Fletcher (1986), Characteristics of the response of sea surface temperature in the central Pacific associated with warm episodes of the Southern Oscillation, *Mon. Weather Rev.*, *114*, 1716–1739, doi:10.1175/1520-0493(1986)114<1716:COTROS>2.0.CO;2.
- Gershunov, A., and T. P. Barnett (1998), Interdecadal modulation of ENSO teleconnections, *Bull. Am. Meteorol. Soc.*, *79*, 2715–2725, doi:10.1175/1520-0477(1998)079<2715:IMOET>2.0.CO;2.
- Halpert, M. S., and C. F. Ropelewski (1992), Surface temperature patterns associated with the Southern Oscillation, *J. Clim.*, *5*, 577–593, doi:10.1175/1520-0442(1992)005<0577:STPAWT>2.0.CO;2.
- Harger, J. R. E. (1995), ENSO variations and drought occurrence in Indonesia and Philippines, *Atmos. Environ.*, *29*, 1943–1955, doi:10.1016/1352-2310(94)00362-O.
- Helsel, D. R., and R. M. Hirsch (1992), *Statistical Methods in Water Resources*, 522 pp., Elsevier, New York.
- Hendon, H. H. (2003), Indonesian rainfall variability: Impacts of ENSO and local air-sea interaction, *J. Clim.*, *16*, 1775–1790, doi:10.1175/1520-0442(2003)016<1775:IRVIOE>2.0.CO;2.
- Hoerling, M. P., A. Kumar, and M. Zhong (1997), El Niño, La Niña, and the nonlinearity of their teleconnections, *J. Clim.*, *10*, 1769–1786, doi:10.1175/1520-0442(1997)010<1769:ENOLNA>2.0.CO;2.
- Janicot, S., V. Moron, and B. Fontaine (1996), Sahel droughts and ENSO dynamics, *Geophys. Res. Lett.*, *23*, 515–518, doi:10.1029/96GL00246.
- Janicot, S., S. Trzaska, and I. Pocard (2001), Summer Sahel-ENSO teleconnection and decadal time scale SST variations, *Clim. Dyn.*, *18*, 303–320, doi:10.1007/s003820100172.
- Ji, L., and A. J. Peters (2003), Assessing vegetation response to drought in the northern Great Plains using vegetation and drought indices, *Remote Sens. Environ.*, *87*, 85–98, doi:10.1016/S0034-4257(03)00174-3.
- Jin, E. K., et al. (2008), Current status of ENSO prediction skill in coupled ocean-atmosphere models, *Clim. Dyn.*, *31*, 647–664, doi:10.1007/s00382-008-0397-3.
- Kahya, E., and J. A. Dracup (1994), The influences of type I El Niño and La Niña events on streamflows in the Pacific southwest of the United States, *J. Clim.*, *7*, 965–976, doi:10.1175/1520-0442(1994)007<0965:TIOTEN>2.0.CO;2.
- Kane, R. P. (2006), Unstable ENSO relationship with Indian regional rainfall, *Int. J. Climatol.*, *26*, 771–783, doi:10.1002/joc.1281.
- Karabörk, M. C., and E. Kahya (2003), The teleconnections between the extreme phases of the Southern Oscillation and precipitation patterns over Turkey, *Int. J. Climatol.*, *23*, 1607–1625, doi:10.1002/joc.958.

- Karabörk, M. C., and E. Kahya (2009), Links between the categorised Southern Oscillation indicators and climate and hydrologic variables in Turkey, *Hydrol. Process.*, *23*, 1927–1936, doi:10.1002/hyp.7331.
- Karabörk, M. C., E. Kahya, and M. Karaca (2005), The influences of the Southern Oscillation and North Atlantic Oscillation on hydrometeorological surface parameters in Turkey, *Hydrol. Process.*, *19*, 1185–1211, doi:10.1002/hyp.5560.
- Karnauskas, K. B., A. Ruiz-Barradas, S. Nigam, and A. J. Busalacchi (2008), North American droughts in ERA-40 global and NCEP North American Regional Reanalyses: A Palmer drought severity index perspective, *J. Clim.*, *21*, 2102–2123, doi:10.1175/2007JCLI1837.1.
- Khan, S., H. F. Gabriel, and T. Rana (2008), Standard precipitation index to track drought and assess impact of rainfall on watertables in irrigation areas, *Irrig. Drain. Syst.*, *22*, 159–177, doi:10.1007/s10795-008-9049-3.
- Kiladis, G. N., and H. F. Diaz (1989), Global climatic anomalies associated with extremes in the Southern Oscillation, *J. Clim.*, *2*, 1069–1090, doi:10.1175/1520-0442(1989)002<1069:GCAAWE>2.0.CO;2.
- Kothawale, D. R., A. A. Munot, and K. K. Kumar (2010), Surface air temperature variability over India during 1901–2007, and its association with ENSO, *Clim. Res.*, *42*, 89–104, doi:10.3354/cr00857.
- Kousky, V. E., M. T. Kagano, S. Iracema, and F. A. Cavalcanti (1984), A review of the Southern Oscillation: Oceanic-atmospheric circulation changes and related rainfall anomalies, *Tellus, Ser. A*, *36*, 490–504, doi:10.1111/j.1600-0870.1984.tb00264.x.
- Lloyd-Hughes, B., and M. A. Saunders (2002), Seasonal prediction of European spring precipitation from El Niño–Southern Oscillation and local sea-surface temperatures, *Int. J. Climatol.*, *22*, 1–14, doi:10.1002/joc.723.
- López-Moreno, J. I., and S. M. Vicente-Serrano (2008), Extreme phases of the wintertime North Atlantic Oscillation and drought occurrence over Europe: A multi-temporal-scale approach, *J. Clim.*, *21*, 1220–1243, doi:10.1175/2007JCLI1739.1.
- Lorenzo-Lacruz, J., S. M. Vicente-Serrano, J. I. López-Moreno, S. Beguería, J. M. García-Ruiz, and J. M. Cuadrat (2010), The impact of droughts and water management on various hydrological systems in the headwaters of the Tagus River (central Spain), *J. Hydrol.*, *386*, 13–26, doi:10.1016/j.jhydrol.2010.01.001.
- Mariotti, A. (2007), How ENSO impacts precipitation in southwest central Asia, *Geophys. Res. Lett.*, *34*, L16706, doi:10.1029/2007GL030078.
- McKee, T. B. N., J. Doesken, and J. Kleist (1993), The relationship of drought frequency and duration to time scales, paper presented at Eighth Conference on Applied Climatology, Am. Meteor. Soc., Anaheim, Calif.
- Meehl, G. A., et al. (2000), An introduction to trends in extreme weather and climate events: Observations, socioeconomic impacts, terrestrial ecological impacts, and model projections, *Bull. Am. Meteorol. Soc.*, *81*, 413–416, doi:10.1175/1520-0477(2000)081<0413:AITIE>2.3.CO;2.
- Mo, K. C. (2000), Relationships between low-frequency variability in the Southern Hemisphere and sea surface temperature anomalies, *J. Clim.*, *13*, 3599–3610, doi:10.1175/1520-0442(2000)013<3599:RBLFVI>2.0.CO;2.
- Mo, K. C., and J. E. Schemm (2008), Relationships between ENSO and drought over the southeastern United States, *Geophys. Res. Lett.*, *35*, L15701, doi:10.1029/2008GL034656.
- Mo, K. C., J. E. Schemm, and S.-H. Yoo (2009), Influence of ENSO and the Atlantic multidecadal oscillation on drought over the United States, *J. Clim.*, *22*, 5962–5982, doi:10.1175/2009JCLI2966.1.
- Nazemosadat, M. J., and A. R. Ghasemi (2004), Quantifying the ENSO-related shifts in the intensity and probability of drought and wet periods in Iran, *J. Clim.*, *17*, 4005–4018, doi:10.1175/1520-0442(2004)017<4005:QTESIT>2.0.CO;2.
- Nel, W. (2009), Rainfall trends in the KwaZulu-Natal Drakensberg region of South Africa during the twentieth century, *Int. J. Climatol.*, *29*, 1634–1641, doi:10.1002/joc.1814.
- New, M., M. Todd, M. Hulme, and P. Jones (2001), Precipitation measurements and trends in the twentieth century, *Int. J. Climatol.*, *21*, 1889–1922, doi:10.1002/joc.680.
- Nicholson, S. E. (2001), Climatic and environmental change in Africa during the last two centuries, *Clim. Res.*, *17*, 123–144, doi:10.3354/cr017123.
- Obasi, G. O. P. (1994), WMO's role in the international decade for natural disaster reduction, *Bull. Am. Meteorol. Soc.*, *75*, 1655–1661, doi:10.1175/1520-0477(1994)075<1655:WRITID>2.0.CO;2.
- Patel, N. R., P. Chopra, and V. K. Dadhwal (2007), Analyzing spatial patterns of meteorological drought using standardized precipitation index, *Meteorol. Appl.*, *14*, 329–336, doi:10.1002/met.33.
- Peters, E., H. A. J. van Lanen, P. J. J. F. Torfs, and G. Bier (2005), Drought in groundwater-drought distribution and performance indicators, *J. Hydrol.*, *306*, 302–317, doi:10.1016/j.jhydrol.2004.09.014.
- Philander, S. G. (1990), *El Niño, La Niña and the Southern Oscillation*, Elsevier, New York.
- Philander, S. G., and A. Fedorov (2003), Is El Niño sporadic or cyclic?, *Annu. Rev. Earth Planet. Sci.*, *31*, 579–594, doi:10.1146/annurev.earth.31.100901.141255.
- Philip, S. Y., and G. J. van Oldenborgh (2009), Significant atmospheric nonlinearities in the ENSO cycle, *J. Clim.*, *22*, 4014–4028, doi:10.1175/2009JCLI2716.1.
- Piechota, T. C., and J. A. Dracup (1996), Drought and regional hydrologic variation in the United States: Associations with the El Niño–Southern Oscillation, *Water Resour. Res.*, *32*, 1359–1373, doi:10.1029/96WR00353.
- Prabhakar, S. V. R. K., and R. Shaw (2008), Climate change adaptation implications for drought risk mitigation: A perspective for India, *Clim. Change*, *88*, 113–130, doi:10.1007/s10584-007-9330-8.
- Quiring, S. M., and S. Ganesh (2010), Evaluating the utility of the Vegetation Condition Index (VCI) for monitoring meteorological drought in Texas, *Agric. For. Meteorol.*, *150*, 330–339, doi:10.1016/j.agrformet.2009.11.015.
- Rajagopalan, B., E. Cook, V. Lall, and B. K. Ray (2000), Spatiotemporal variability of ENSO and SST teleconnections to summer drought over the United States during the Twentieth Century, *J. Clim.*, *13*, 4244–4255, doi:10.1175/1520-0442(2000)013<4244:SVOEAS>2.0.CO;2.
- Rasmusson, E. M., and T. M. Carpenter (1982), Variations in tropical sea surface temperature and surface wind fields associated with the Southern Oscillation/El Niño, *Mon. Weather Rev.*, *110*, 354–384, doi:10.1175/1520-0493(1982)110<0354:VITSS>2.0.CO;2.
- Rayner, N. A., D. E. Parker, E. B. Horton, C. K. Folland, L. V. Alexander, D. P. Rowell, E. C. Kent, and A. Kaplan (2003), Global analyses of sea surface temperature, sea ice, and night marine air temperature since the late nineteenth century, *J. Geophys. Res.*, *108*(D14), 4407, doi:10.1029/2002JD002670.
- Redmond, K. T., and R. W. Koch (1991), Surface climate and streamflow variability in the Western United States and their relationship to large-scale circulation indices, *Water Resour. Res.*, *27*, 2381–2399, doi:10.1029/91WR00690.
- Richard, Y., N. Fauchereau, I. Poccarr, M. Rouault, and S. Trzaska (2001), 20th century droughts in southern Africa: Spatial and temporal variability, teleconnections with oceanic and atmospheric conditions, *Int. J. Climatol.*, *21*, 873–885, doi:10.1002/joc.656.
- Roegner, E., J. M. Oberhuber, A. Bacher, M. Christoph, and I. Kirchner (1996), ENSO variability and atmospheric response in a global coupled atmosphere–ocean GCM, *Clim. Dyn.*, *12*, 737–754, doi:10.1007/s003820050140.
- Ropelewski, C. F., and M. S. Halpert (1986), North American precipitation and temperature patterns associated with the El Niño/Southern Oscillation (ENSO), *Mon. Weather Rev.*, *114*, 2352–2362, doi:10.1175/1520-0493(1986)114<2352:NAPATP>2.0.CO;2.
- Ropelewski, C. F., and M. S. Halpert (1987), Global and regional scale precipitation patterns associated with the El Niño/Southern Oscillation, *Mon. Weather Rev.*, *115*, 1606–1626, doi:10.1175/1520-0493(1987)115<1606:GARSPP>2.0.CO;2.
- Ropelewski, C. F., and M. S. Halpert (1989), Precipitation patterns associated with the high index phase of the Southern Oscillation, *J. Clim.*, *2*, 268–284, doi:10.1175/1520-0442(1989)002<0268:PPAWTH>2.0.CO;2.
- Ropelewski, C. F., and M. S. Halpert (1996), Quantifying Southern Oscillation–precipitation relationships, *J. Clim.*, *9*, 1043–1059, doi:10.1175/1520-0442(1996)009<1043:QSOPR>2.0.CO;2.
- Rouault, M., and Y. Richard (2005), Intensity and spatial extent of droughts in southern Africa, *Geophys. Res. Lett.*, *32*, L15702, doi:10.1029/2005GL022436.
- Schonher, T., and S. E. Nicholson (1989), The relationship between California rainfall and ENSO events, *J. Clim.*, *2*, 1258–1269, doi:10.1175/1520-0442(1989)002<1258:TRBCRA>2.0.CO;2.
- Schubert, S., R. Koster, M. Hoerling, R. Seager, D. Lettenmaier, A. Kumar, and D. Gutzler (2007), Predicting drought on seasonal-to-decadal time scales, *Bull. Am. Meteorol. Soc.*, *88*, 1625–1630, doi:10.1175/BAMS-88-10-1625.
- Shabbar, A., and W. Skinner (2004), Summer drought patterns in Canada and the relationship to global sea surface temperatures, *J. Clim.*, *17*, 2866–2880, doi:10.1175/1520-0442(2004)017<2866:SDPICA>2.0.CO;2.
- Sheffield, J., K. M. Andreadis, E. F. Wood, and D. P. Lettenmaier (2009), Global and continental drought in the second half of the twentieth century: Severity-area-duration analysis and temporal variability of large-scale events, *J. Clim.*, *22*, 1962–1981, doi:10.1175/2008JCLI2722.1.
- Siegel, S., and N. J. Castellan (1988), *Nonparametric Statistics for the Behavioral Sciences*, McGraw-Hill, New York.

- Smith, T. M., and R. W. Reynolds (2004), Improved extended reconstruction of SST (1854–1997), *J. Clim.*, *17*, 2466–2477, doi:10.1175/1520-0442(2004)017<2466:IEROS>2.0.CO;2.
- Smith, T. M., and C. F. Ropelewski (1997), Quantifying Southern Oscillation–precipitation relationships on atmospheric GCM, *J. Clim.*, *10*, 2277–2284, doi:10.1175/1520-0442(1997)010<2277:QSOPRF>2.0.CO;2.
- Sterl, A., G. J. van Oldenborgh, W. Hazeleger, and G. Burgers (2007), On the robustness of ENSO teleconnections, *Clim. Dyn.*, *29*, 469–485, doi:10.1007/s00382-007-0251-z.
- Stone, R. C., G. L. Hammer, and T. Marcussen (1996), Prediction of global rainfall probabilities using phases of the Southern Oscillation Index, *Nature*, *384*, 252–255, doi:10.1038/384252a0.
- Svoboda, M., et al. (2002), The drought monitor, *Bull. Am. Meteorol. Soc.*, *83*, 1181–1190.
- Svoboda, M. D., M. J. Hayes, D. A. Wilhite, and T. Tadesse (2004), Recent advances in drought monitoring, paper presented at 14th Conference on Applied Climatology, Am. Meteorol. Soc., Seattle, Wash.
- Szalai, S., C. S. Szinell, and J. Zoboki (2000), Drought monitoring in Hungary, in *Early Warning Systems for Drought Preparedness and Drought Management*, pp. 182–199, World Meteorol. Org., Geneva, Switzerland.
- Tippett, M. K., and A. G. Barnston (2008), Skill of multimodel ENSO probability forecasts, *Mon. Weather Rev.*, *136*, 3933–3946, doi:10.1175/2008MWR2431.1.
- Trenberth, K. E. (1997), The definition of El Niño, *Bull. Am. Meteorol. Soc.*, *78*, 2771–2777, doi:10.1175/1520-0477(1997)078<2771:TDOENO>2.0.CO;2.
- Trenberth, K. E., and C. J. Guillemot (1996), Physical processes involved in the 1988 drought and 1993 floods in North America, *J. Clim.*, *9*, 1288–1298, doi:10.1175/1520-0442(1996)009<1288:PPITD>2.0.CO;2.
- Trenberth, K. E., and T. J. Hoar (1996), The 1990–1995 El Niño–Southern Oscillation event: Longest on record, *Geophys. Res. Lett.*, *23*, 57–60, doi:10.1029/95GL03602.
- United Nations (2008), Trends in sustainable development: Agriculture, rural development, land, desertification and drought, report, Dep. of Econ. and Social Affairs, New York.
- Vicente-Serrano, S. M. (2005), El Niño and La Niña influence on drought conditions at different time scales in the Iberian Peninsula, *Water Resour. Res.*, *41*, W12415, doi:10.1029/2004WR003908.
- Vicente-Serrano, S. M. (2007), Evaluating the impact of drought using remote sensing in a Mediterranean, semi-arid region, *Nat. Hazards*, *40*, 173–208, doi:10.1007/s11069-006-0009-7.
- Vicente-Serrano, S. M., and J. I. López-Moreno (2005), Hydrological response to different time scales of climatological drought: An evaluation of the standardized precipitation index in a mountainous Mediterranean basin, *Hydrol. Earth Syst. Sci.*, *9*, 523–533, doi:10.5194/hess-9-523-2005.
- Vicente-Serrano, S. M., S. Beguería, and J. I. López-Moreno (2010a), A multi-scalar drought index sensitive to global warming: The Standardized Precipitation Evapotranspiration Index–SPEI, *J. Clim.*, *23*, 1696–1718, doi:10.1175/2009JCLI2909.1.
- Vicente-Serrano, S. M., S. Beguería, J. I. López-Moreno, M. Angulo, and A. El Kenawy (2010b), A new global 0.5° gridded dataset (1901–2006) of a multiscale drought index: Comparison with current drought index datasets based on the Palmer Drought Severity Index, *J. Hydrometeorol.*, *11*, 1033–1043, doi:10.1175/2010JHM1224.1.
- Vidal, J.-P., E. Martin, L. Franchistéguy, F. Habets, J.-M. Soubeyroux, M. Blanchard, and M. Baillon (2010), Multilevel and multiscale drought reanalysis over France with the Safran–Isba–Modcou hydrometeorological suite, *Hydrol. Earth Syst. Sci.*, *14*(3), 459–478, doi:10.5194/hess-14-459-2010.
- Wilhite, D. A. (1996), A methodology for drought preparedness, *Nat. Hazards*, *13*, 229–252, doi:10.1007/BF00215817.
- Wilhite, D. A., M. D. Svoboda, and M. J. Hayes (2007), Understanding the complex impacts of drought: A key to enhancing drought mitigation and preparedness, *Water Resour. Manage.*, *21*, 763–774, doi:10.1007/s11269-006-9076-5.
- Wu, R., and B. P. Kirtman (2006), Changes in spread and predictability associated with ENSO in an ensemble coupled GCM, *J. Clim.*, *19*, 4378–4396, doi:10.1175/JCLI3872.1.

C. Azorin-Molina, J. Lorenzo-Lacruz, E. Morán-Tejeda, J. I. López-Moreno, and S. Vicente-Serrano, Instituto Pirenaico de Ecología, CSIC, Campus de Aula Dei, PO Box 202, E-50080 Zaragoza, Spain. (svicen@ipe.csic.es)

S. Beguería, Estación Experimental de Aula Dei, CSIC, Avda. Montañana 1005, E-50080 Zaragoza, Spain.

L. Gimeno and R. Nieto, Environmental Physics Laboratory, Universidade de Vigo, E-32004 Ourense, Spain.